Distribution Agreement

In presenting this thesis or dissertation as a partial fulfillment of the requirements for an advanced degree from Emory University, I hereby grant to Emory University and its agents the non-exclusive license to archive, make accessible, and display my thesis or dissertation in whole or in part in all forms of media, now or hereafter known, including display on the world wide web. I understand that I may select some access restrictions as part of the online submission of this thesis or dissertation. I retain all ownership rights to the copyright of the thesis or dissertation. I also retain the right to use in future works (such as articles or books) all or part of this thesis or dissertation.

Signature:

_____ _____

James E. Davidheiser Date

Characterization of Chaotic Motion in a Rotating Drum

By

James E. Davidheiser

Doctor of Philosophy, Physics

(Eric Weeks)

Advisor

(Stefan Boettcher)

Committee Member

(Vincent Huynh)

Committee Member

(Michael Schatz)

Committee Member

(Kurt Warncke)

Committee Member

Accepted:

(Lisa A. Tedesco, Ph.D.)

Dean of the Graduate School

(Date)

Characterization of Chaotic Motion in a Rotating Drum

By

James E. Davidheiser

B.S., Drexel University, 2002

Advisor: Eric R. Weeks, Ph.D.

An abstract of a dissertation

submitted to the Faculty of the

Graduate School of Emory University

in partial fulfillment of the requirements for the degree of

Doctor of Philosophy in Physics

2009

Abstract

Characterization of Chaotic Motion in a Rotating Drum

By

James E. Davidheiser

Numerous studies in the past have demonstrated the potential for geometrically simple fluid systems to produce complicated dynamical behavior. In particular, small collections of non-Brownian particles moving within viscous fluids can follow chaotic trajectories. In this work, we study a rotating drum filled with pure glycerol and three large, heavy particles.

In studying these rotating drum systems, we have found a rich and varied phase space, made up of several previously unseen behaviors. With varying rotation rate, the particles can undergo straightforward cascading periodic behavior, and grouped periodic cascades we have labeled as doublet and triplet states. Furthermore, we find two regimes of qualitatively distinct chaotic behavior, with one type biased to either side of the drum, and the other lacking bias.

The rotating drum experiment serves as a simple model system to demonstrate chaotic behavior in fluid dynamical systems. The existence of such model systems gives a baseline to which other systems can be compared and better understood, and our use of robust, easily implemented measurements serves as a straightforward comparison point which can be applied to various other chaotic fluid systems.

Characterization of Chaotic Motion in a Rotating Drum

By

James E. Davidheiser

B.S., Drexel University, 2002

Advisor: Eric R. Weeks, Ph.D.

A dissertation submitted to the Faculty of the

Graduate School of Emory University

in partial fulfillment of the requirements for the degree of

Doctor of Philosophy in Physics

2009

Acknowledgements

A dissertation is an undertaking that simply cannot be accomplished alone. Without the help and support of so many people, I would not have ever made it to this point. Thanks to my adviser, Eric Weeks, for his insight and guidance in undertaking this long journey, and to all of the Weeks group for welcoming me into the lab. Thanks to Stefan Boettcher for giving me my first taste of real research, and for giving me the motivation and opportunity to come to work at Emory in the first place. The rest of my committee members - Michael Schatz, Vincent Huynh, and Kurt Warncke - provided valuable insights into the underlying physical relevance when I was buried in experimental details. Cody Anderson and Horace Dale from the machine shop, and Jon Carr from the electronics shop provided invaluable help completing the real work of getting the experimental apparatus built and operational - without their help this experiment would have never been more than an idea.

My family all helped me take on this goal, but I am especially grateful to my parents, James and Terry Davidheiser, who have always taken pride in my academic pursuits, and to my grandmother, Mary Davidheiser, whose support gave me the opportunity to go after my dream of becoming a physicist. Without all of your help over the years, I wouldn't be where I am today.

And last but not least, to my wonderful fiancee Amy - no matter how difficult things have seemed, your constant love and care made the impossible seem possible. I couldn't have done this without you.

Contents

List of Figures

Chapter 1

Introduction

1.1 Motivation

In the study of classical Newtonian chaotic systems, there are certain fundamental example systems which have been heavily studied and which are used as examples to which other systems can be compared. Simple experiments such as a billiard ball on a stadium-shaped table [1] or a forced pendulum [2] are easily constructed laboratory experiments which can be studied in depth to better understand the fundamental properties of low dimensional chaotic behavior in these classical systems.

Fluid dynamics, while significantly complicated by the continuum nature of its governing equations, also contains such fundamental experiments. Much as the simple gravitational three-body problem [3] can serve as a useful tool to study low dimensional chaos resulting from Newton's equations, the fluid three-body problem can serve the same purpose for understanding chaos resulting from the Navier-Stokes equations.

There are a host of these geometrically simple fluids experiments which can yield interesting results and give us insight into the character of chaotic fluid dynamical systems, but we focus specifically on the question of groups of particles sedimenting under the influence of gravity. When these groups of particles are large ($N \gg 1$), we

see bulk sedimentation effects, including various interesting swirls and vortices [4]. However, when N is small, interesting effects are still seen, with the potential for small numbers of particles interacting through the fluid to exhibit chaotic behavior.

Due to experimental considerations which will be discussed in this Chapter, we limit our study to the motion of small collections of particles moving within a rotating drum filled with viscous fluid. Figure 1.1 shows a cartoon picture of the type of experiment on which we will focus, where we use three large, non-Brownian beads. When the drum rotates, these beads undergo a periodic cascade in the vertical direction. Due to the viscous nature of the fluid, the beads feel long-range interactions due to the fluid. At certain rotation rates, they can also wander erratically in the horizontal direction, with seemingly random-like trajectories. We will focus our discussion on the relation between the fluid interactions and bead trajectories, and also provide both qualitative and quantitative measurements to describe the nature of the particles' horizontal motion.

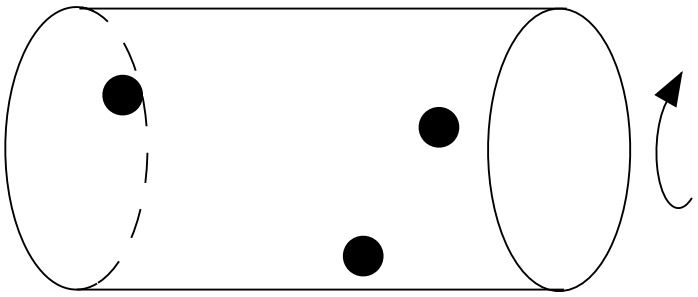

Figure 1.1: We study a rotating drum filled with viscous fluid and three beads. These beads are dragged upwards by the front wall of the drum until gravity pulls them away from the wall and they fall through the fluid. This periodic cascading in the vertical direction can often lead to interesting horizontal motion.

This system serves as an analogue for simple sedimentation experiments, with the constraint that the rotation of the drum forces the three beads to remain close together, continually interacting. By doing so, we ensure that the behavior of the beads has the potential to remain persistent, allowing us to study it over a long period of time and describe the motion of a single state in great detail.

By understanding the chaotic motions of a small collection of beads interacting through a fluid flow, we contribute to a base of knowledge about these simple model fluid systems, which can serve as examples against which other, more complicated behavior is compared, just as in the classical Newtonian examples.

1.2 The Stokeslet Model

The complex behaviors present in systems involving fluid dynamics provide a rich variety of interesting physical systems to study. The non-linearity of the Navier-Stokes equation is responsible for both the mathematical difficulty of fluid dynamics and the complexity and variety of fluid dynamical phenomena [5]. There are many approaches that can be taken to study fluid interactions, both experimentally and theoretically. One such approach is to deal with particles moving within fluid. For particles that are large and heavy enough, the fluid will influence the motion of the particles, but the particles will have enough inertia that they don't exactly follow the fluid flow. This can allow us to study the particle motion while somewhat abstracting away the exact details of the fluid dynamics. In this case, the fluid can be treated as a source of long-range interaction between the particles.

As an example of this approach, we consider the Stokeslet model, which uses the approximation given in the Stokes equations, reasonable when fluid inertia is unimportant compared to viscosity [6]:

$$\vec{\nabla} \cdot \vec{u} = 0, \tag{1.1}$$

$$-\vec{\nabla} p + \mu \Delta \vec{u} + \vec{f} = 0, \tag{1.2}$$

where μ is the dynamic viscosity, $\vec{u} = \vec{u}(\vec{r})$ is the fluid velocity field, $p = p(\vec{r})$ is the pressure field, and $\vec{f} = \vec{f}(\vec{r})$ is the local force field. Equation 1.1 tells us the fluid is incompressible, while Eqn. 1.2 is the Navier-Stokes equation with inertial

terms neglected, so only the viscous terms contribute. The model then approximates the velocity field due to a single particle of radius a moving with velocity $\vec{v}_0$ in an unbounded fluid as

$$\vec{u}(\vec{r}) = av_0\vec{U}(\vec{r}), \quad r > a, \tag{1.3}$$

$$\vec{U}(\vec{r}) = \left(\frac{\vec{e}}{r} + \frac{(\vec{e}\cdot\vec{r})\vec{r}}{r^3}\right), \tag{1.4}$$

where $\vec{e}$ is a unit vector in the direction of the particle velocity $\vec{v}$. If we consider particles moving under the influence of gravity, such as those during the falling portion of our drum experiment, the steady-state sedimentation velocity of an isolated particle, $v_0 = F_g/(6\pi\mu a)$ can be used in place of v_0 in the above equations.

Since the Stokes equations are linear, this method allows one to approximate the velocity of a given particle as a superposition of the velocity fields of the other particles, such that

$$\dot{\vec{r}}_i = \vec{v}_0 + av_0 \sum_{j\neq i} \vec{U}(\vec{r}_i - \vec{r}_j). \tag{1.5}$$

This model demonstrates how it is possible to simplify the nonlinear Navier-Stokes equations into a more manageable representation where each particle is treated as acting under the influence of potentials resulting from the motion of the other particles. While our experiment takes place within a regime where both viscosity and inertia are important, invalidating the simplifications of the Stokeslet model, conceptually similar ideas will be used throughout this Chapter to look at groups of particles interacting via some long-range fluid effects, while mostly disregarding the exact details of the fluid behavior.

1.3 Chaotic Motion

In Sec. 1.1, we alluded to random-like movement of particles. By random-like, we specifically mean deterministic chaos, hereafter referred to as simply chaos. A deterministic chaotic system is one that, while deterministic in nature (that is, a set of initial conditions has only a single possible outcome), appears random in behavior [7]. There are two main properties which describe chaotic dynamical systems: exponential sensitivity to initial conditions, and topological mixing.

Exponential sensitivity to initial conditions is one of the most commonly referenced characteristics of chaotic behavior, conceptualized by the popular idea of the "butterfly effect", first popularized by E. Lorenz at the December 1972 meeting of the American Association for the Advancement of Sciences in his talk titled ""Predictability- Does the Flap of a Butterfly's Wings in Brazil Set Off a Tornado in Texas? [8]". This example proposes that, due to the extreme sensitivity to initial conditions in the equations which govern weather, a flap of a butterfly's wings could change initial conditions enough to drastically alter the outcome of the system. In more technical terms, a small perturbation in the initial conditions of a dynamical system, advanced forward in time, can produce an exponential divergence of the trajectory of that system in the phase space comprised of all relevant variables in the system. This exponential divergence with slightly different initial conditions is a hallmark of chaotic behavior.

Topological mixing describes mixing in which, if you select any two regions of phase space, and follow them forward in time, they will eventually overlap. While this is a more difficult behavior to quantify directly, its more fundamental meaning serves as inspiration for much of the analysis to be done in Ch. 4. On a qualitative level, topological mixing describes how a system explores phase space - a chaotic system will tend to explore phase space more thoroughly than a periodic one, regardless of its initial conditions. Due to the lack of delicate control over initial conditions in our

own experiments, this concept will drive our analysis of the rotating drum system.

To support our claim that the behavior seen in our system is chaotic in nature, we will explore several analogous works which demonstrate chaotic behavior in simple particle-fluid systems. In addition to those explored in the next several sections, various other experiments and simulations have shown that particles interacting with fluids can behave chaotically. Shin and Maxey found that non-spherical particles settling in a fluid flow field exhibited chaotic motion [9]. In a similar vein, Anil Kumar et al. demonstrated chaotic dynamics in the behavior of spheroids in a simple flow with periodic external forcing [10]. Aref and Balachandar demonstrated that stirring particles in a fluid can also produce chaotic results [11]. Indeed, many studies have illustrated chaotic behavior in a variety of situations, including effects such as fluid flow field, external forcing, Brownian diffusion, and hydrodynamic interactions [12]. In this Chapter, we will look at a subset of chaotic behaviors, those involving particles sedimenting under the influence of a constant external force (i.e. gravity).

1.4 Chaos in Pure Sedimentation

In early sedimentation experiments [13], it was demonstrated that the interaction between non-Brownian particles sedimenting in liquid can be chaotic. Specifically, if three particles were released close to each other, it was seen that two of the particles would pair up and travel together, while the third particle would move on its own unique trajectory. The remarkable result, however, was that this pairing was sensitive to initial conditions. If the starting positions of the three particles (labeled 1, 2, and 3) were at a given configuration, particles 1 and 2 might pair up. Changing this configuration slightly, however, might cause particles 1 and 3 to pair.

This work was further analyzed computationally by Jánosi et al [14] for the Stokeslet theoretical model described in Sec. 1.2. Two example trajectories, illus-

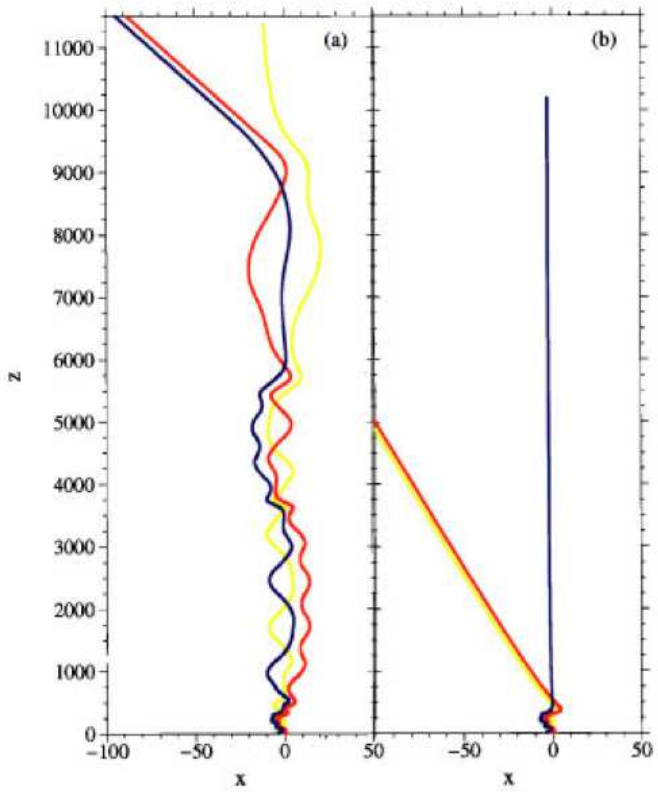

Figure 1.2: Example trajectories for particles starting at z=0 with x positions (a) (-3.9050,-1.0,1.0) and (b) (-3.9048, -1.0, 1.0) are plotted. Sedimentation occurs in the positive z direction for this simulation. Note that the particle left behind and the escape time are very different, despite the closeness of the original positions in phase space. This suggests exponential sensitivity to initial conditions. Image taken from Ref. [14].

trating sensitivity to initial conditions, are shown in Fig. 1.2. Due to the simplicity of this model and the power of modern computers, it was possible to sample *millions* of initial starting configurations. An example of the results is given in Fig. 1.3. In this figure, the results of simulations with various starting configurations are shown. The positions of two of the particles are held fixed, with the x and z positions of the third (test) particle varied, and the particles allowed to sediment in the z direction. Color on the graph indicate which of the three particles was left behind: red regions indicate that particle 1 was left behind, yellow particle 2, and blue regions indicate that the test particle was left behind. There is a rich fractal structure to this image,

the details of which are beyond the scope of this Dissertation, but the complex structure of the initial condition space gives a clear indication of chaotic behavior, serving as a concrete example of a simple chaotic system consisting of particles sedimenting within fluid.

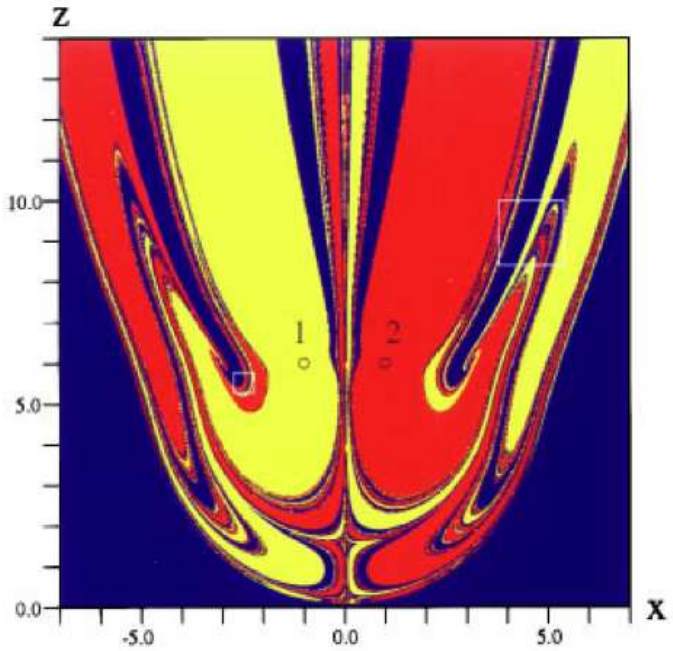

Figure 1.3: Here we see a section of initial configuration space of the test particle. Particles 1 and 2 always start from the same positions, while the axes show the starting position of the test particle. Eventually, two of the three particles will pair up, and leave the third particle behind. Colors indicate which particle was left behind. Red, particle 1; yellow, particle 2; blue, test particle. Note the self-similar, complex structure of this configuration space. Image taken from Ref. [14].

In many ways, this simple system illustrates the purest picture of sedimentation dynamics and how chaos can arise in these situations. However, the Stokeslet model used for the simulations is only valid in the limit where viscosity completely dominates behavior, and fluid inertia has no effect. The relative contributions of these two forces can be defined as the Reynolds number, $Re = UL/\nu$, where U is a characteristic velocity, ν is the kinematic viscosity, and L is a characteristic length. $Re \gg 1$ corresponds with an inertia-dominated flow, while flows with $Re \ll 1$ are dominated

by viscosity. As most computational models use approximations only valid within certain ranges of Reynolds numbers, we will explore chaotic behavior with an experimental study, rather than a simulation, so that parameters can be varied smoothly between different regimes.

The execution of the Jánosi experiment in a laboratory setting poses many obstacles. The most obvious of these is the fact that it's impractical to sample millions of initial configurations in the lab. Therefore, we would have much trouble showing a rich set of initial conditions as illustrated in Fig. 1.3. Furthermore, as seen in Fig. 1.2, the chaotic mixing occurs during some finite time, after which straight line trajectories set in, and therefore the chaotic behavior is transient, meaning limited in time. The fact that there there is no phase space in which the particle trajectories are bounded tells us that there are no periodic orbits, and thus the characterization of the route to chaos would be more difficult. If we could instead find a system where the motion is bounded, and the system settles into a specific subset of phase space, we could study the properties of that bounded phase space, known as an attractor [15], using a rich set of existing tools. Perhaps the most appealing feature of an attractor is that, for many initial conditions, even lying outside the attractor, the long-term behavior of the system will be to settle into the attractor and remain trapped there. From an experimental standpoint, this means we can study the features of the chaotic behavior of the system without the requirement of extremely precise control of initial conditions. Instead, we can focus our efforts on controlling the parameters of the system to look for an onset of chaotic behavior when these parameters are varied.

1.5 Orbits and Bounded Behavior in Sedimentation

As we saw, a fundamental experimental difficulty of the pure sedimentation problem is that the motion is unbounded. However, Aidun and Ding [16] illustrated, again computationally, that it is possible to construct a sedimentation experiment in which bounded periodic orbits, and a transition to bounded chaos with varied parameters, can be found.

In their simulation, Aidun and Ding considered two dimensional sedimentation of circular cylinders in a narrow channel. In this case, the width of the channel was only four times the diameter of the cylinders, so that wall effects were very important. Perhaps the most vital characteristic of this experiment, however, is the fact that the wall effects constrain the particles in a way that wall interactions allow chaotic behavior to occur with only two particles. Thus, there is no concern that pairing will allow a particle to be left behind, resulting in transient behavior. In order to probe the dependence of chaotic behavior on Reynolds number, Aidun and Ding varied the magnitude of the external gravitational force, which in turn varied the velocity U of the particles and the Reynolds number $Re = UL/\nu$

Because the chaotic behavior for this system is not transient, it is possible to construct a phase space which illustrates the dynamics of the system with a minimum of variables. This phase space was defined by the distance between each particle and the side wall, y_1/d and y_2/d. At low Reynolds numbers, the system shows a periodic trajectory, with an example phase space shown in Fig. 1.4a. As the Reynolds number is increased, the dynamics transition into a more complex period two orbit as shown in Fig. 1.4b. At even higher Reynolds number, they find chaotic behavior as shown in Fig. 1.4c.

This simulation gives us evidence that the trajectory of a sedimenting system

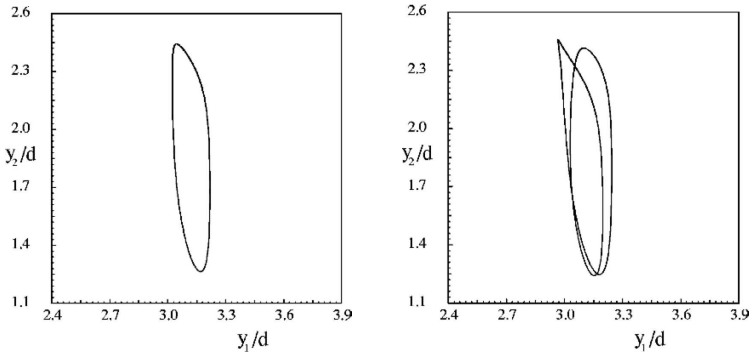

(a) Period One

(b) Period Two

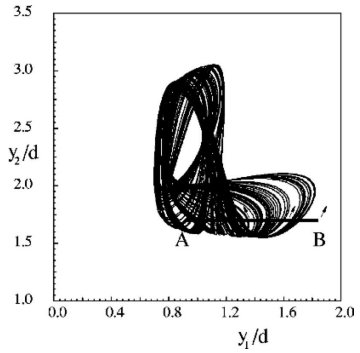

(c) Chaos

Figure 1.4: This plot contains trajectories of circular cylinders in phase space illustrating a transition from periodic behavior to chaos. At low Reynolds number, the particles oscillate periodically in phase space (a). As Re is increased, the system undergoes a period doubling, so that the particles now oscillate with period two (b). This increase in complexity eventually leads to a chaotic state at high enough Reynolds number. (c). Image taken from Ref. [16].

can be bounded in phase space and produce chaotic behavior. However, it is again an impractical experimental setup for the lab. In the simulation, the sedimentation occurs in an infinite-height channel, which is obviously impossible to replicate physically. Furthermore, Aidun and Ding controlled the Reynolds number by holding the viscosity and density ratio fixed and varying the external (gravitational) force. While convenient from a computational standpoint, such unphysical techniques are impractical in a laboratory setting.

1.6 The Rotating Drum

If we now consider three dimensional beads moving through a fluid at moderate Reynolds number, they can interact through long-range fluid interactions brought about by their fluid wakes [17]. The numerical studies carried out in Ref. [17] showed that the wakes of two identical spherical particles held side-by-side can interact in such a way as to cause an effective force between those two particles. Specifically, when the two particles are close enough together, the effective force is a repulsion between the two particles. As they move apart, this force diminishes until it crosses zero and becomes an attractive force, with a peak in this attractive force at a distance of ~ 5 particle diameters d, and a decreasing force as distance increases beyond $\sim 5d$, with force essentially equal to zero around $\sim 20d$.

Mullin, et al. [18] demonstrated a physical experiment that illustrates how these wake interactions can cause chaotic particle motion within a fluid. They studied a hollow cylinder, filled with glycerine, oriented horizontally, and rotated at various angular speeds ω. When one or two beads were placed within this container, fixed-point, periodic, or solid-body behavior was found, depending on the particle Reynolds number, defined $Re_p = \omega r_c r_b/\nu$, where r_c and r_b are the radii of the cylinder and ball, and ν is the kinematic viscosity of the glycerol. No chaotic behavior was observed when

there were only one or two beads. When three beads were placed within the container, however, low dimensional chaos, in addition to the aforementioned behaviors, was observed over well-defined ranges of Re.

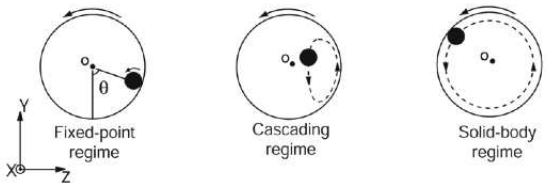

(a) (b) (c)

Figure 1.5: There are three regimes of possible behavior for a single bead in a rotating drum. At low rotation rate, the bead rotates in a fixed position on the wall of the drum. At higher rotation rates, this bead cascades in the y-z plane. At significantly high rotation rates, the bead is fixed in position on the drum wall by centrifugal force. Image taken from Ref. [18]

For two beads, at a low rotation rate, the system illustrated a steady state behavior, where the beads stayed at a stationary position and rotated with the cylinder, as shown in Fig. 1.5a. As ω was increased, the system moved into a time-dependent cascading regime, where each bead is dragged up along the side of the cylinder, until it falls away from the wall and lands further down, before being dragged up again (Fig. 1.5b). In this regime, the two beads were in a stable anti-phase configuration - when one bead was at the top of the cascade cycle, the other was at the bottom, and vice versa. At high enough ω, the beads rotate along with the cylinder, firmly planted to the wall, in a solid-body regime (Fig. 1.5c). These various regimes are demarcated by certain rotation rates ω, and thus by certain values of the Reynolds number Re.

For the three bead case, there is again fixed-point behavior, where the beads were completely independent of each other, at $\mathrm{Re} < 1.21$. At $1.21 < \mathrm{Re} < 2.12$, the beads illustrated cascading behavior in the $y - z$ plane with the x positions fixed. It was noted that the outer beads were again stably out of phase with each other, and the middle bead was at an intermediate position between the two. At $\mathrm{Re} = 2.12$ there

was a reversible transition to a chaotic regime where the particles started to wander erratically in the horizontal (x) direction while still cascading in the $y - z$ plane. A typical sample of a 400-second time series of the x position of the three beads is shown in Fig. 1.6. At Re = 4.53, there was a transition to solid body motion.

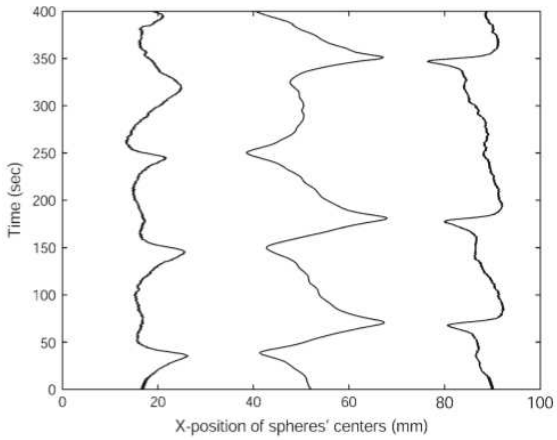

Figure 1.6: Mullin plotted x component time series for the positions of the three beads. The smallest gaps between the series are the same as the bead diameter and thus represent the closest approach of the beads. [18]

In this work, Mullin demonstrated a simple, tabletop experiment where chaotic behavior occurs in a geometry which shares several parallels with simple sedimentation experiments. The motion is completely bounded in phase space by the presence of the drum walls, forcing the particles to remain within a range in which there is potential for them to interact with one another, neatly avoiding the experimental difficulties discussed previously in this Chapter. This experiment serves as the inspiration for our own study. We find that the rotating drum is a useful investigative tool, which allows us to study a persistent chaotic state. This chaotic state is stable over long timescales, allowing the collection of large amounts of data. The rest of this dissertation will focus on our own efforts to understand and study the three-particle rotating drum problem in greater detail than was discussed by Mullin. We will demonstrate several new behaviors, and provide a description of a rich and interesting phase space, along with quantitative measurements of the properties of trajectories.

Chapter 2

Theory

2.1 Motivation

This Chapter will focus on the theory of viscous fluid within a rotating drum. The motivation for this discussion is to provide evidence that the interesting behavior we observe is due not to the rotation of the drum directly, but rather to the fluid motion that occurs as a result of the beads' motion relative to the bulk flow of the fluid. The theory discussed in this Chapter is borrowed heavily from Ref. [19], which in turn draws from several introductory texts [20, 21, 22, 5].

2.2 Equations of Motion

Written in a rotating frame of reference with rotation $\vec{\omega}$, the Navier-Stokes equation is given by

$$\frac{D\vec{u}}{Dt} = -\frac{1}{\rho}\vec{\nabla}p + \nu\nabla^2\vec{u} - 2\vec{\omega}\times\vec{u} - \vec{\omega}\times(\vec{\omega}\times\vec{r}), \tag{2.1}$$

where $\vec{u}(\vec{r},t)$ is the velocity field of a fluid of density ρ with kinematic viscosity η. $D\vec{u}/Dt$ is the advective term, and it is equal to the sum of terms due to pressure p, dissipation due to viscosity ν, Coriolis and centripetal forces. In cylindrical coordi-

nates, with $\vec{\omega} = \omega\hat{z}$, the centripetal term can be written as the gradient of a scalar, $-\vec{\omega}\times(\vec{\omega}\times\vec{r}) = (1/2)\vec{\nabla}(\vec{\omega}\times\vec{r})^2 = (1/2)\vec{\nabla}(\omega^2 r^2)$, and thus combined with the pressure term to give

$$\frac{D\vec{u}}{Dt} = -\frac{1}{\rho}\vec{\nabla}[p - (1/2)\rho\omega^2 r^2] + \nu\nabla^2\vec{u} - 2\vec{\omega}\times\vec{u}, \tag{2.2}$$

or if we define an effective pressure $p' = p - (1/2)\rho\omega^2 r^2$,

$$\frac{D\vec{u}}{Dt} = -\frac{1}{\rho}\vec{\nabla}p' + \nu\nabla^2\vec{u} - 2\vec{\omega}\times\vec{u}. \tag{2.3}$$

We can nondimensionalize Eqn. 2.3 using a characteristic length L, velocity U, time L/U, and pressure P, such that $u^* = u/U$, $p^* = p'/P$, $t^* = Ut/L$, and $\vec{\nabla} = \vec{\nabla}/L$, to give

$$\frac{U}{\omega L}\frac{D\vec{u}^*}{Dt^*} = -\frac{P}{\rho U L\omega}\vec{\nabla}^* p^* + \frac{\nu}{\omega L^2}\nabla^{*2}\vec{u}^* - 2\hat{z}\times\vec{u}^*. \tag{2.4}$$

Dropping the asterisks, we further define the nondimensional Rossby number $Ro \equiv U/(\omega L)$ and the nondimensional Ekman number $Ek \equiv \nu/(\omega L^2)$, and rewrite the Navier-Stokes equation:

$$Ro\frac{D\vec{u}}{Dt} = -Ro\left(\frac{P}{\rho U^2}\right)\vec{\nabla}p + Ek\nabla^2\vec{u} - 2\hat{z}\times\vec{u}. \tag{2.5}$$

Here the Rossby number gives the relative importance of advection compared to the Coriolis force, and the Ekman number tells us the ratio of viscous dissipation to Coriolis force. The two together help characterize the behavior of rotating flows.

2.3 Drum Spin-Up

If we consider a drum filled with glycerine, such as that in Sec. 1.6, initially stationary in the lab frame, which is very quickly accelerated to a constant rotation rate ω, the

viscous fluid within that drum will not accelerate instantaneously.

In the rotating frame, initially the fluid will appear to be rotating in the opposite direction from $\vec{\omega}$, with a maximum velocity $U = \omega r_c$. Here, the Rossby number can be defined:

$$Ro = \frac{U}{\omega r_c} = \frac{\omega r_c}{\omega r_c} = 1. \tag{2.6}$$

In cases of Rossby number of $O(1)$, the spin-up time of fluid within a drum is determined by the Ekman pumping time τ_E [23].

2.3.1 Ekman Pumping

If we consider the Ekman number for the fluid within the drum,

$$Ek = \frac{\nu}{\omega L^2} = \frac{\nu}{\omega {r_c}^2} \sim 0.02 - 0.05, \tag{2.7}$$

we note that, in the bulk of the fluid, during spin-up, Coriolis forces play a far more important role than viscous forces. This role takes the form of Ekman pumping at the end caps of the cylinder, providing damping which drives the rotating flow.

If we consider flow very near the cylinder end caps, the no-slip boundary condition requires that the fluid be motionless within the rotating reference frame. Thus, there must be some transitional layer over which the fluid transitions from its bulk flow to what is happening at the end caps. If we call the length scale of this layer δ_E, we can define an Ekman number based on this length scale. Over the length of this layer, viscous dissipation must be able to take the fluid from the bulk velocity to the boundary velocity, meaning $Ek \sim 1$. Thus, we can write the typical thickness of the Ekman layer as

$$\delta_E \sim \sqrt{\nu/(\omega)}. \tag{2.8}$$

This Ekman boundary layer has an additional effect on the flow within the cylinder. The layer will draw fluid from high-pressure regions (those rotating in the opposite direction from the drum), and inject it into low-pressure regions. If there are two Ekman layers, one at each end of the cylinder, separated by a distance h_0, this cyclic pumping causes an overall damping effect $\vec{u(t)} \sim \vec{u_o} e^{-t/\tau_E}$ where τ_E is the Ekman time:

$$\tau_E = \frac{h_0}{\sqrt{\nu\omega}}. \tag{2.9}$$

This damping effect will tend to damp out any motion within the rotating frame, bringing fluid that was at rest in the lab up to the rotation rate of the cylinder. For our experiment, with $\omega \sim 5 - 13$ rad/s, $\delta_E \sim 1.0 - 1.8$ cm. With a calculated $h_0 \sim l_c - 2\delta_E$, we find that for our typical rotation rates, $\tau_E \sim 2.4 - 3.7$ s. This implies that the behavior seen in our measurements, lasting several hours in duration, is not dependent on effects from the initial spin-up of the drum fluid.

2.4 Fluid Effects Due to Beads Moving Within the Drum

If we now consider the introduction of beads into the drum, observed at a time $t \gg \tau_e$, we consider the effect their motion will have on perturbations about the solid-body fluid motion stabilised after the spin-up time τ_E. When we are within the cascade regime, the beads will repeatedly cascade in the $y - z$ plane, being dragged up the front wall of the cylinder, then falling away from it and falling through the cylinder, as illustrated in Fig. 2.1

We recorded approximate values for v_{up} and v_{down} for many values of ω and plotted v vs ωr_c in Fig. 2.2. The solid line drawn at $v = \omega r_c$ shows an upper limit to the

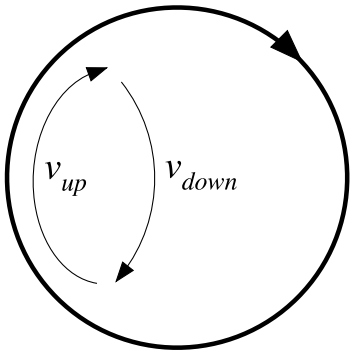

Figure 2.1: Looking in along the rotational axis of the drum, the beads will be dragged upwards along the cylinder wall with a velocity v_{up} and then fall through the fluid at a velocity v_{down}.

cascade velocity in the lab frame. As these beads are cascading within the lab frame, their maximum velocity in the rotation frame would be if they fall along the radial direction $\hat{r}$, so the maximum velocity in the rotating frame is equal to the maximum velocity in the lab frame. Thus, we can define $U = \omega r_c$, and our Rossby number for the fluid motion resulting from the motion of the beads within the rotating reference frame is again equal to unity. This implies that we can treat the system overall as beads sedimenting within a fluid, and neglect Coriolis forces in their behavior. The lack of Coriolis influence tells us that the motion of the beads is driven not by the rotation of the drum, but by the long-range fluid interactions caused by the bead motions within the drum.

Since our Rossby number is the same as in the spin-up case, there will still be an Ekman damping effect, which serves to damp out fluid flow which is different from the bulk flow in the drum. However, this damping effect has little influence on the interesting particle motion in the horizontal direction. In Sec 4.4, we will show that typical times for the collisions between particles are of order $\tau_{col} \sim 100$s, two orders of magnitude removed from the Ekman time $\tau_E \sim 1$s. Similarly, the particle turnover time, that is the time for a single cascade to occur, is of order 1s.

However, despite the fact that the Ekman time is shorter than the the time scale of the interactions we study, Ekman pumping has an important influence on the

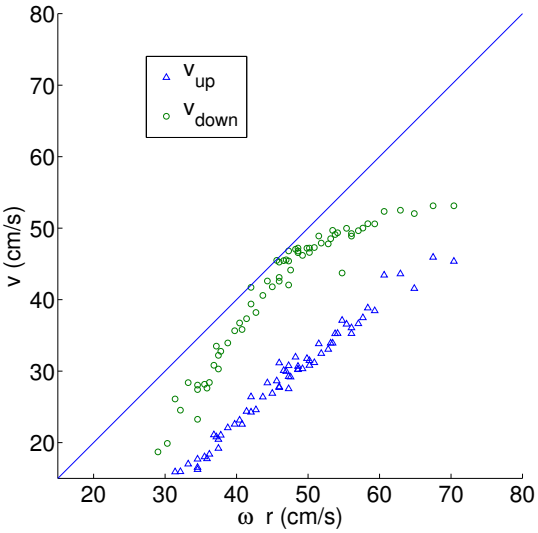

Figure 2.2: Cascade velocities v_{up} and v_{down} are plotted versus ωr_c for a variety of rotation rates. The solid line represents $v = \omega r_c$, showing that ωr_c is an upper bound for the cascade velocities.

system's behavior. In Sec. 2.3.1, we calculated the typical thickness of the Ekman layer $\delta_E \sim 1 - 1.8$ cm. This pumping layer provides an effective boundary layer which the beads don't cross, and which repels the beads if they begin to intrude. This can be observed in experiments, where the particles are seen to never approach within less than a centimeter or so of the end caps.

2.5 Particle-Particle Interactions

In order to better understand the source of the particle-particle interactions, we consider the particles' effects on fluid flow, in the form of wakes which radiate horizontally within the drum. In either reference frame, the velocity of the bead, $v_b \sim \omega r_c$ is determined by the rotation rate of the cylinder. Since we have determined that the particle motion is not heavily influenced by the drum rotation, we consider the particle Reynolds number $Re = UL/\nu$, which determines the contribution of fluid inertial effects relative to viscous drag. For a cascading bead of diameter $2r_b$, the Reynolds number is:

$$Re = \frac{\omega r_c r_b}{\nu} \sim 5 - 15. \tag{2.10}$$

This corresponds to a laminar flow where both viscosity and fluid inertia play a role in the fluid flow. In order to quantify whether viscous forces play a role in the horizontal motions of the beads, we consider the typical viscous damping time $\tau_\nu \sim L^2/\nu$. For interactions of particles across the length $l_d = 25$ cm of the drum, $\tau_\nu \sim 80$ s, on the same order as the particle interaction time $\tau_{col} \sim 100$ s.

If we consider the ratio of inertial forces for the particles compared to the fluid, we can typify the relative contributions by comparing the density ratio $\rho_b/\rho_f \sim 6.2$, which implies that fluid inertia will have less influence upon the bead trajectories than the Reynolds number might otherwise imply. Due to their large inertia relative to the fluid, the beads will not tend to follow fluid streamlines exactly, but rather interact via drag.

2.6 Gravitational Force

To this point, we have limited our discussion to motion within the rotating drum without directly mentioning the influence due to gravity. The presence of gravity can be seen indirectly through the use of the cascade velocity U, which is a result of the force of gravity on the beads. However, in order to study its effect more directly, we define the Galilei number, which is the ratio of gravitational to viscous forces. With the force due to gravity defined as $F_g = (4/3)\pi r_b^3 \Delta\rho g$, and the viscous drag defined as the Stokes drag $F_\nu = 6\pi\nu r_b U$, we can define the Galilei number [24]

$$Ga = \frac{F_g}{F_\nu} = \frac{2r_b^2 \Delta\rho g}{9\nu U} \sim 1.3 - 3.9 \tag{2.11}$$

With $Ga = 3.9$ for $\omega = 5$ rad/s and $Ga = 1.3$ for $\omega = 15$ rad/s. This shows

that the influence due to gravity is always comparable to that due to viscous drag, which is not surprising, as most motion within the rotating frame of reference is due to the gravity-driven cascade. At lower rotation rates, the force due to gravity is proportionally large, meaning the cascade will have a smaller amplitude, as observed, while at higher rotation rates, the forces due to gravity and viscous drag are equal in magnitude, leading to large amplitude cascades.

2.7 Summary

In the prior discussion, we defined the Rossby and Ekman numbers, which describe the contributions of advection and viscous dissipation, respectively, compared to the Coriolis force. Considering the spin-up of the drum, $Ro \sim 1$ and $Ek \sim 0.02 - 0.05$, implying that Coriolis and inertial forces dominate the initial spin-up behavior. However, the time scale of this spin up is very short, on the order of a few seconds, implying that the initial spin-up has little influence on the long-term behavior of the system. Furthermore, once we introduce beads into the system, we find that the rotational effects have little influence on the interesting behavior of the system, which is dominated by viscous forces on a timescale two orders of magnitude larger than the timescales of rotational forces. We summarize the experimental parameters used in this experiment in Table 2.1, and their resultant dimensionless numbers and time

l_c	25 cm	Length of cylinder
r_c	5.71 cm	Radius of cylinder
r_b	0.795 cm	Radius of bead
ω	$5 - 13$ rad/s	Rotation rate of cylinder
T	24.7 ± 0.1°C	Temperature
ρ_f	1.26 g/cm^3	Fluid density
ρ_b	7.65 g/cm^3	Bead density
ν	7.69 St (cm^2/s)	Kinematic viscosity $\nu = \mu/\rho$
μ	968 cP	Dynamic viscosity

Table 2.1: Summary of important variables in the rotating drum experiment

and length scales in Table 2.2.

Ro	$\frac{U}{\omega L} \leq \frac{r_c}{2L}$	1
Ek	$\frac{\nu}{\omega L^2}$	$0.02 - 0.05$
Re_b	$\frac{UL}{\nu} = \frac{\omega r_c r_b}{\nu}$	$5 - 15$
τ_E	$\frac{h_0}{\sqrt{\nu\omega}}$	$2.4 - 3.6$ s
δ_E	$\sqrt{\nu/(\omega)}$	$1.0 - 1.8$ cm
τ_{col}	(measured)	~ 100s
$\tau_{cascade}$	(measured)	~ 1 s
τ_ν	L^2/ν	80 s

Table 2.2: Summary of dimensionless numbers in the rotating drum experiment

Chapter 3

Instrumentation and Methods

3.1 Experimental Apparatus

3.1.1 The Drum

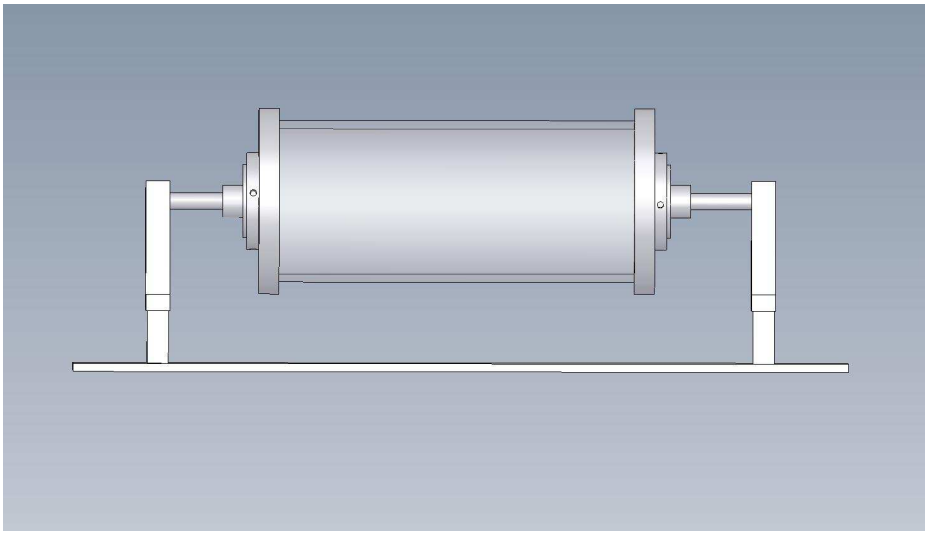

Figure 3.1: The drum, shown looking in from a side view, is placed on a stand which allows it to rotate about the horizontal axis.

The experimental apparatus consists of a 25 cm long horizontally oriented sealed drum, with an inner diameter of 11.43 cm, as shown in Fig. 3.1. The main body of the drum is constructed from a section of acrylic glass pipe with a wall thickness of $\sim$ 1 cm. To each end of this drum, waterproof threaded aluminum caps are fitted.

Each cap has an shaft attached via an adjustable mounting, so that the shaft can be carefully centered within the cap. These shafts attach to a stand via two bearings, which allow the drum to rotate freely about the horizontal axis. The base of the drum stand contains four adjustment screws for leveling the apparatus.

On one of the drum shafts, a pulley is mounted, and connected via a belt to a Dayton 1/2 HP 3-phase A/C motor driven by a Fuji AF-300 controller. This allows the drum to be rotated on its axis at a variable rotation rate ω over a range from $\sim 5 - 13$ rad/s. Due to the belt drive connection, the actual motor rotation rate is potentially different from that displayed on the control box, so the rotation rate of the drum is measured independently using a Pasco PS-2120 rotary motion sensor connected to a computer. Stability measurements taken over a four-hour period show the rotation rate to be stable to within 1%. As all experiments are started from rest, we also measure the time for the drum to spin up to within 1% of its final velocity, and find typical spin-up times to be on the order of tens of seconds.

The apparatus, in its current form, has two limitations on rotation rate. At rotation rates much below ~ 5 rad/s, the motor begins to "stutter", without the smooth, constant rotation rates needed for the experiment. This could be corrected by choosing appropriate pulley ratios, but as will be shown in Sec. 4.2, little interesting behavior occurs at these low speeds. Similarly, there is an upper limit on the rotation rate, but this limitation is due to the physical construction of the device. The bearings used are non-lubricated and begin to heat up significantly at higher rotation rates. However, these high rotation rates are again regimes where little interesting behavior occurs.

The drum is filled with 99.5% pure glycerol from Sigma-Aldrich, and three 440c stainless steel ball bearings from Winstead Precision Ball Company with a diameter of 1.59 cm, density $\rho_b = 7.65 \times 10^3$ kg/m^3, and weight of 16.1 grams. When immersed in glycerol ($\rho_f = 1.26 \times 10^3$ kg/m^2), the beads have an apparent buoyant weight of

13.4 grams each.

3.1.2 Temperature Control

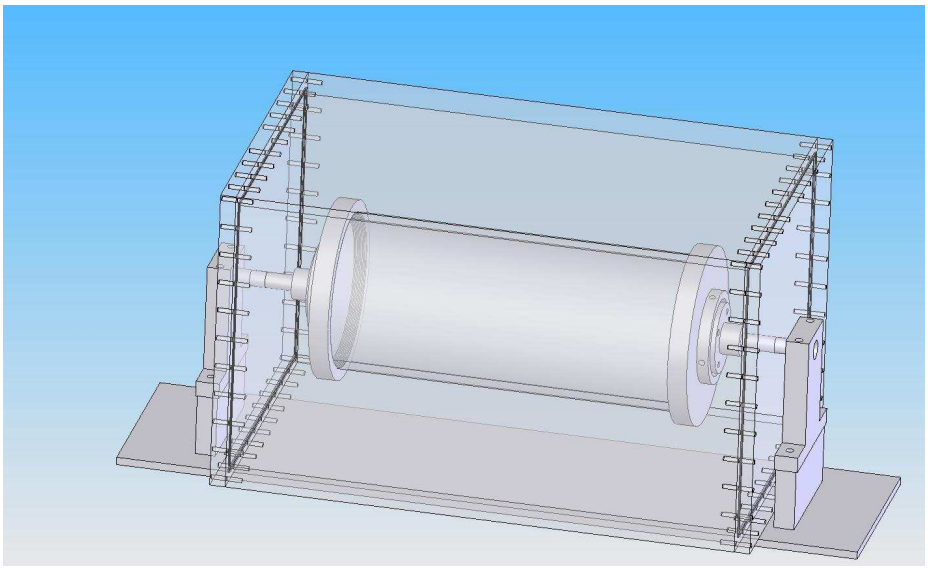

Figure 3.2: The drum is immersed in water, which is temperature controlled via a copper heat exchanger connected to a recirculating digital temperature control bath. The tank is built from acrylic glass, open on top, with the two end caps held on with screws and sealed with an o-ring and silicone paste.

It is well-known that the viscosity of glycerol is strongly dependent on temperature [25]. Thus, in order to maintain constant viscosity, it is necessary to control the temperature of the fluid within the drum. To do so, we immerse the drum in a tank of water, shown in Fig. 3.2, in which a copper heat exchanger has been placed. We connect this heat exchanger to a Thermo NESLAB RTE-7 digital refrigerated/heated bath, which is maintained at 25° C in all experiments. The rotation of the drum provides sufficient mixing to allow the water within the tank to be maintained at 24.7±0.1° C, as measured by a digital thermometer, independently for each experiment. This results in a measured kinematic viscosity $\nu = 7.69$ Stokes.

3.1.3 Imaging

In order to study the behavior of the particles as the drum is rotated, we need to track their motion. To do so, we use a Pixelink PL-B741F 1.3 megapixel firewire monochromatic camera connected to a personal computer running Windows XP. Attached to the camera is an Edmund Optics NT56-788 megapixel lens with a fixed focal length of 16 mm.

Under normal ambient lighting, there is significant motion blur associated with the fast-moving particles. To minimize this, a Monarch Instruments Nova-Strobe DAX is used to light the particles from behind, with an opaque screen surrounding the entire apparatus to block ambient light. The strobe is attached to a foil reflector box with a bead-blasted acrylic glass window, which serves as a diffuser to provide uniform light distribution. To ensure that the firing of the strobe is synchronized with the shutter of the camera, a General Purpose Output interface on the camera is programmed to output a current sink pulse each time the shutter on the camera opens. The circuit shown in Fig. 3.3 is used to convert that output pulse to a TTL-level signal, which can be input into the strobe's external trigger port. This provides the needed lighting conditions for crisp, clear images with no motion blur.

The experiments conducted last for up to six hours, significantly longer than the included OEM software for the camera is able to record. Due to this, it was necessary to write a custom video capture package, which can capture the raw camera data, convert it into image data in memory, and stream those images directly to a compressed video file. The completed software package is discussed in more detail in Appendix A.

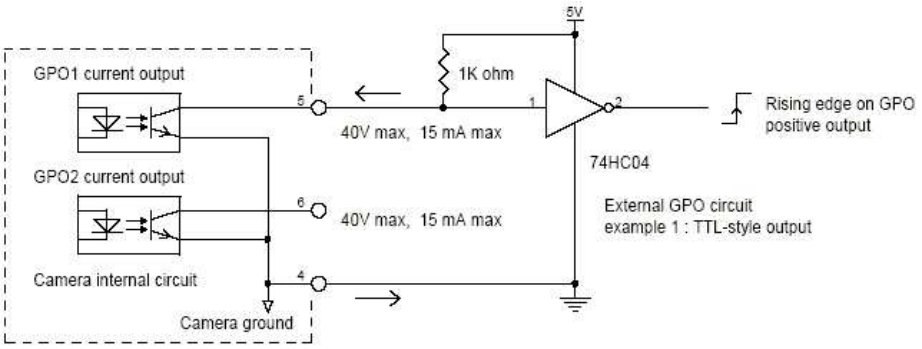

Figure 3.3: Circuit to connect camera General Purpose Output to strobe trigger input. The Pixelink GPO is an open collector current sink interface, which acts as either an an open circuit (no connection to anything) or a short circuit to ground. This current sink is connected through a pull-up resistor to a 5 V source, in parallel with a NOT gate. When the GPO is off, no current can flow through it, and current will instead flow to node 1, meaning node 1 is on. When the GPO is switched on, all the current flows through the GPO to ground, and node 1 is now off. Since node 1 is connected to a NOT gate, off at node 1 corresponds to on at node 2, and vice versa. Thus, when the GPO sink is turned off, there will be no current output from the circuit, and when the GPO is switched on, there will be a 5 V voltage output at node 2. This corresponds to a rising-edge TTL signal, which can be fed directly into the Nova-Strobe trigger input, such that every time the GPO is switched on, the strobe will fire [26]. Figure taken from Pixelink product documentation [27].

3.2 Particle Tracking Software

3.2.1 Algorithm

In order to analytically study the behavior of the particles moving within the rotating drum, we developed a Matlab-based tracking algorithm. Matlab was chosen due to an existing rich set of tools already developed for the platform which greatly simplify testing new algorithms and data analysis methods.

This algorithm is simple to execute from a programming standpoint, as it takes advantage of very fast built-in functions in the Matlab environment. In total, over five million frames of video are analyzed, so it is vital to use as efficient an algorithm as possible, so that data can be analyzed in a reasonable amount of time and used as a guide to determine what data still needs to be collected. The following method was chosen after comparing several different algorithms, as the heavy use of built-in functions gave the fastest run times of the tested algorithms.

The algorithm requires the backlighting of the particles, so they appear as dark objects on a bright background. Due to the highly reflective surface of the stainless steel ball bearings, reflections would prove problematic for image analysis if there were any ambient light apart from the backlighting.

There are four main steps in the algorithm:

1. Load frame

   A frame is loaded from the compressed .avi video file and stored in Matlab as a matrix of greyscale pixel values (a bitmap). This original image is shown in Fig. 3.4a.

2. Convert to binary

   The Matlab IM2BW() command is applied to the bitmap with a given threshold, so that all pixels with an intensity below this threshold value will be set to an

intensity of 0, while all above will be set to an intensity of 1, producing a binary bitmap. The result of this operation is shown in Fig. 3.4b.

3. Area Detection

   The binary image is inverted, so that all dark areas become light, and vice versa. This makes it so that the beads are shown as light objects on a dark background. This inverted image is fed into BWAREAOPEN(IMAGE,P) , which is an efficient, highly optimized Matlab command which morphologically opens a binary image. That is, it removes all continuous regions of light pixels ("objects") with fewer than P pixels.

   This command removes imperfections in the image, such as dark areas near the edges of the cell, air bubbles, and smudges on the surface, which might otherwise give false positives. The result of this operation, shown in Fig. 3.4c, demonstrates the removal of the imaging artifacts seen in Fig. 3.4b.

4. Labeling of objects

   BWLABEL(IMAGE) is a Matlab command which labels the continuous regions within the image. It returns an $N \times N$ matrix L the same size as the binary image, with all background pixels having a value of 0, all pixels within the first object a value of 1, all those within the second a value of 2, and so on.

5. Location of objects

   The labeled matrix L contains separate labeled regions corresponding to each of the beads within the drum. In order to locate the centers of the beads, the command REGIONPROPS(L,'CENTROID') is used. This is another Matlab image analysis tool, which measures various properties of labeled image regions. In this case, it computes the centroid of the labeled region, which identifies the center of mass of each particle. The centers of mass are returned as a standard Matlab structure containing x and y coordinates in pixels for each bead, which

are plotted on the original image Fig. 3.4d for illustration purposes.

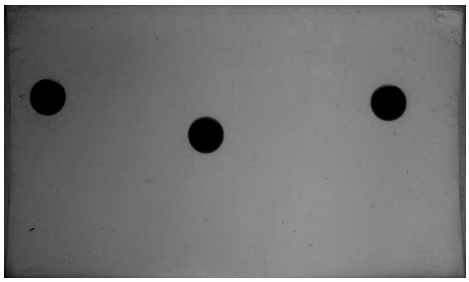

(a) Original back-lit image of beads in drum

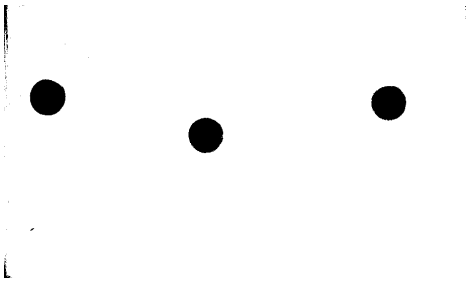

(b) Image after binary thresholding

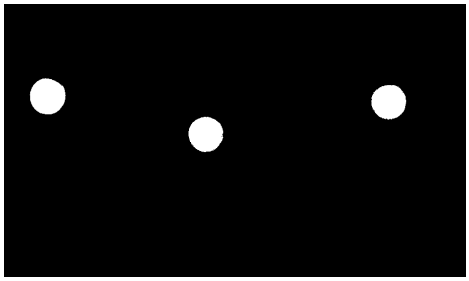

(c) Image after application of BWAREAOPEN()

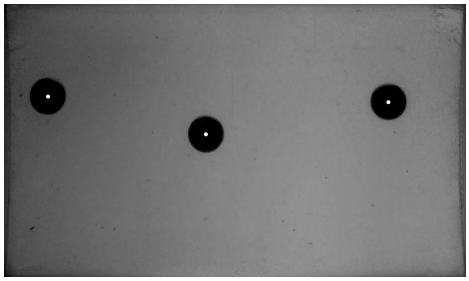

(d) Tracked positions plotted on top of original image

Figure 3.4: The four primary steps in the image analysis algorithm were carried out in Matlab. The original greyscale image shows dark beads on a bright background. The image is converted to binary (step b) with a set threshold, then a filter is applied to remove background smudges and imperfections (c). Finally, the centers of the individual objects are located, and their positions plotted over the original image for verification.

3.2.2 Notes and limitations

It should be noted that there are numerous other algorithms available which carry out particle tracking on collections of particles. However, many of these algorithms are geared toward microscopy, which generally involves objects that are only a few pixels across. In this experiment, beads are $\sim 10^2$ pixels across, and many microscopy-focused algorithms tend to slow down significantly as the size of the objects increases. Also, when a particle is $\sim 10^1$ pixels across, sub-pixel accuracy is far more important for obtaining particle positions as accurately as possible. For the rotating drum, noise in particle positions, described in the next paragraph, is larger than a single pixel,

and so negates the usefulness of such calculations for sub-pixel measurements. Due to all of these considerations, the chosen algorithm was better suited for analysis of particle trajectories.

The system contains inherent distortion noise due to the multiple optical interfaces within the apparatus. Light coming from around the beads within the glycerol (index of refraction $i = 1.47$) must pass through the curved front surface of the acrylic drum ($i = 1.49$) into water ($i = 1.33$), through another layer of acrylic, and then into air ($i = 1$). Passing between these interfaces, most notably the curved drum surface, causes refraction which distorts the positions of the particles as seen by the camera. Due to the proximity of the camera to the front of the cell, this effect is exaggerated when the beads are near the end caps of the drum, and minimized when the beads are near the center. This noise is periodic in nature, and corresponds to the cascading of the beads within the drum. When beads are being dragged up along the front drum wall, there is little distortion. However, when the beads fall away from the wall in the cascade motion, their positions are distorted more. At worst case, the distortion gives an uncertainty of $\pm 0.1 r_b$. Note that here we see an additional benefit of the temperature control bath. If we were to remove the bath, the interface would be acrylic/air at the drum surface, with a larger difference in i and thus a greater distortion effect.

While this uncertainty sounds somewhat high at first glance, our analysis is intentionally focused on techniques in which exact particle positions are unimportant. Furthermore, during experiments in which the beads move in the horizontal direction, they vary in position by several particle diameters, so the noise is small in comparison. In most of our analysis, time is more important than exact particle position, and the noise occurs at a high frequency (dictated by drum rotation rate) that is not comparable to the timescales of interesting behavior within the system.

From a technical standpoint, this algorithm has one significant flaw. BWLABEL

defines objects based on their connectivity, not their shape. Therefore, if two beads are touching, when back-lit they will look like one continuous blob, and be detected as a single object, rather than a pair of beads. In hindsight, it would have been preferable to account for this consideration in the algorithm, but for the sake of programming simplicity at the time, the code simply discards those frames of video where fewer than three beads were detected. As the beads are constantly moving and colliding, beads rarely stay in contact for more than a few frames, and so interpolation was used to fill in the "missing" frames where the beads overlapped.

Since the algorithm is unable to identify the beads when they are touching, it is also unable to track the beads when they cross over one another. If two beads collide, depending on the type of the collision and the positions of the the individual beads, they can potentially cross over one another, swapping places. This does not show up in the particle tracking, as there is no way to identify individual beads when they are back-lit with no features to differentiate them from one another. Again, however, since our analysis techniques focus on characterizing collisions and the distances between particles, the exact definition of which particle is which becomes less important.

Chapter 4

Results and Analysis

4.1 Data Collection

In order to study the behavior of the particles at different rotation rates, we recorded a total of $\sim$ 5.75 million frames of video, at 5 frames per second, corresponding to approximately 320 hours of video recorded. The lengths of individual experiments ranged from tens of minutes up to six hours, depending on the needs of that given experiment.

For each experiment, we first initialized the particle positions by setting the drum rotation rate ω to that of a known chaotic state, and stopping the drum when the three beads were distributed equidistant from one another, with approximately 3.5 particle diameters spacing between the beads,. The exact rotation rate was not important, as it was simply used as a tool to position the particles. Once the drum was stopped and enough time allowed to elapse for any fluid motion to cease, we first started the rotation of the motor, and immediately began recording video. Videos were streamed directly to the PC hard drive into a compressed Xvid MPEG-4 AVI file. Video files were then analyzed using the Matlab software discussed in Sec. 3.2.1.

4.2 Phase Diagram

4.2.1 Description of the Five Phases

We found five distinct types of behavior within the cascade regime described in Sec. 1.6. With the axes defined as drawn in Fig 4.1, at the lowest rotation rates, the three beads simply cascade in the $y - z$ plane with no significant motion in the horizontal (x) direction. Figure 4.2 shows a typical example of this periodic trajectory, at a rotation $\omega = 5.31$ rad/s.

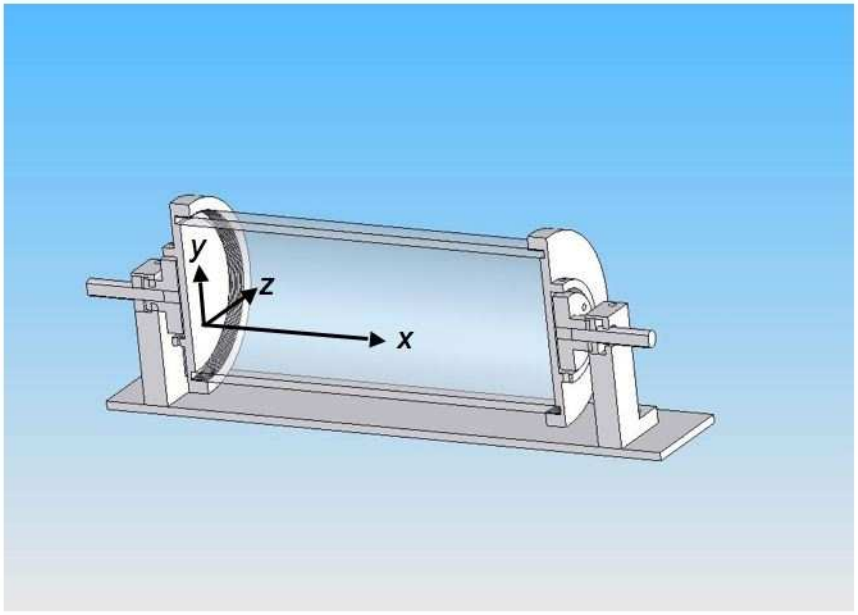

Figure 4.1: The axes are defined such that x represents the horizontal direction, y is the vertical, and z is the depth away from the front edge of the drum. Note that, with the current apparatus, there is no way to measure z directly.

As rotation rate is increased beyond this initial simple periodic regime, there are several possible types of trajectories, depending on rotation rate. The two simplest of these are also periodic, but to differentiate their unique behaviors we have labeled them as doublet (Fig. 4.3) and triplet (Fig. 4.4) states.

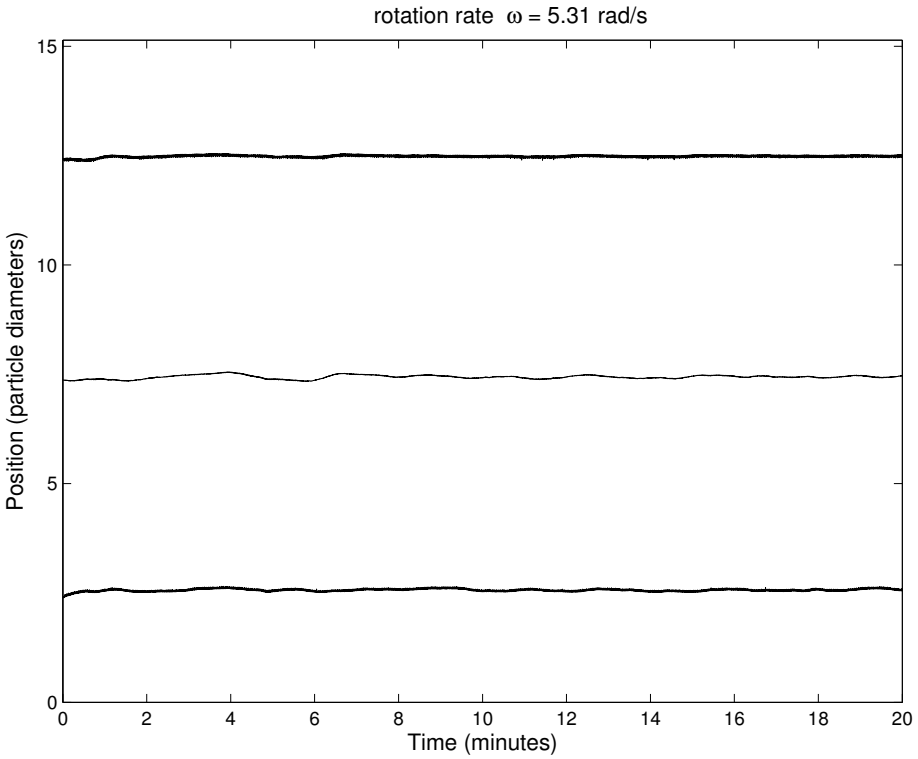

Figure 4.2: Horizontal positions of the three particles are plotted versus time in minutes. Positions are normalized by the diameter of the beads, and the limits of the position axis correspond to the end caps of the drum. Here we see a typical periodic trajectory, where the only variation of the horizontal particle positions is due to experimental noise. We call this periodic because, in the vertical direction, the particles are cascading in a periodic fashion determined by the rotation rate of the drum. These simple periodic behaviors only occur at very low rotation rates.

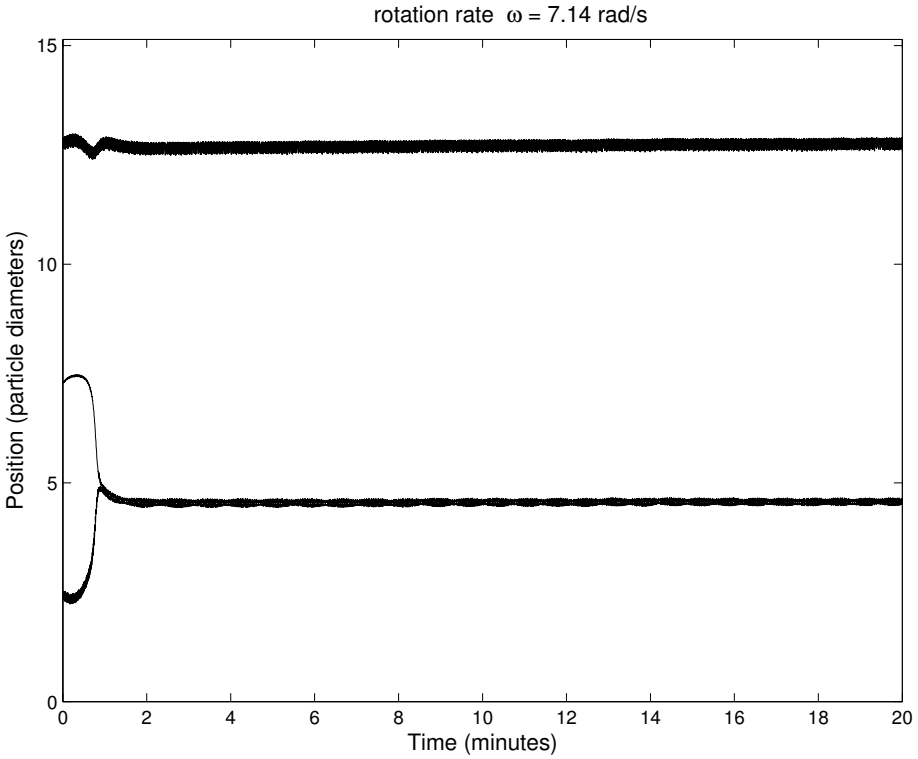

Figure 4.3: At $\omega = 7.14$ rad/s, the three beads form a typical doublet state. Very quickly after the rotation of the drum is started, two of the three beads come together and form a pair, which is stable in time. These beads will cascade in line with one another with no apparent interaction with the third bead. The determination of which two beads come together is seemingly random, implying sensitivity to the exact initial conditions. Due to the lack of ability to control initial positions with any precision, it is difficult to test this, but a pair is always formed at this rotation rate ω.

In the doublet state, two of the beads will lock together so that they are cascading in one another's wakes. The determination of which two beads will tend to pair up is a result of initial conditions, and not a systematic trend in the experimental apparatus. Simply stopping and restarting the drum at the same rotation rate can sometimes switch which two beads will form a pair.

In the triplet state, all three beads come together and cascade in line with one another, in a similar fashion to the doublet state. The three beads can be stacked on top of each other, touching, or they can be spaced out within the drum, following each others' wakes without touching. Both the doublet and triplet states are stable

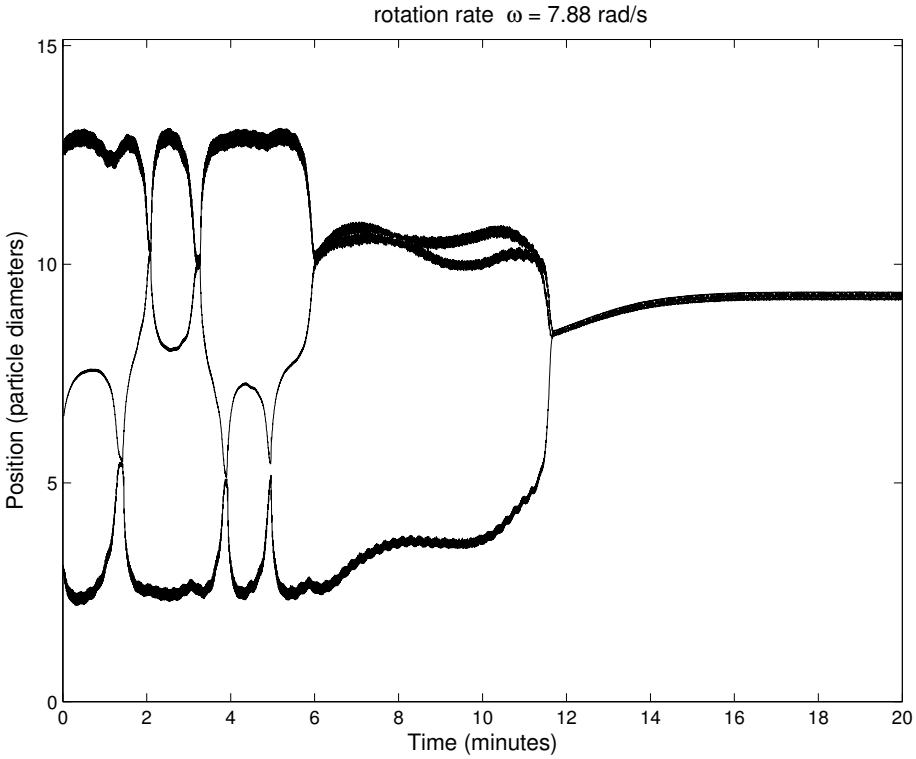

Figure 4.4: In the triplet state, all three beads come together and cascade in line with one another. This is a stable configuration.

configurations and have been tested to remain locked for periods exceeding twenty-four hours in duration.

At certain rotation rates, the beads will wander chaotically in the x direction. For chaotic trajectories with a low enough ω, there will be a bias to one side of the drum or the other. This biased chaotic trajectory is illustrated by a typical example as shown in Fig. 4.5. Two of the three beads will tend to repeatedly collide with one another, while the third bead will remain segregated at the far end of the drum. This third bead still experiences long range forces from the other two beads, and can be seen to move in phase with the collisions of the other two. The determination of which two beads will tend to pair up is again seemingly a result of initial conditions, analogous to the doublet state.

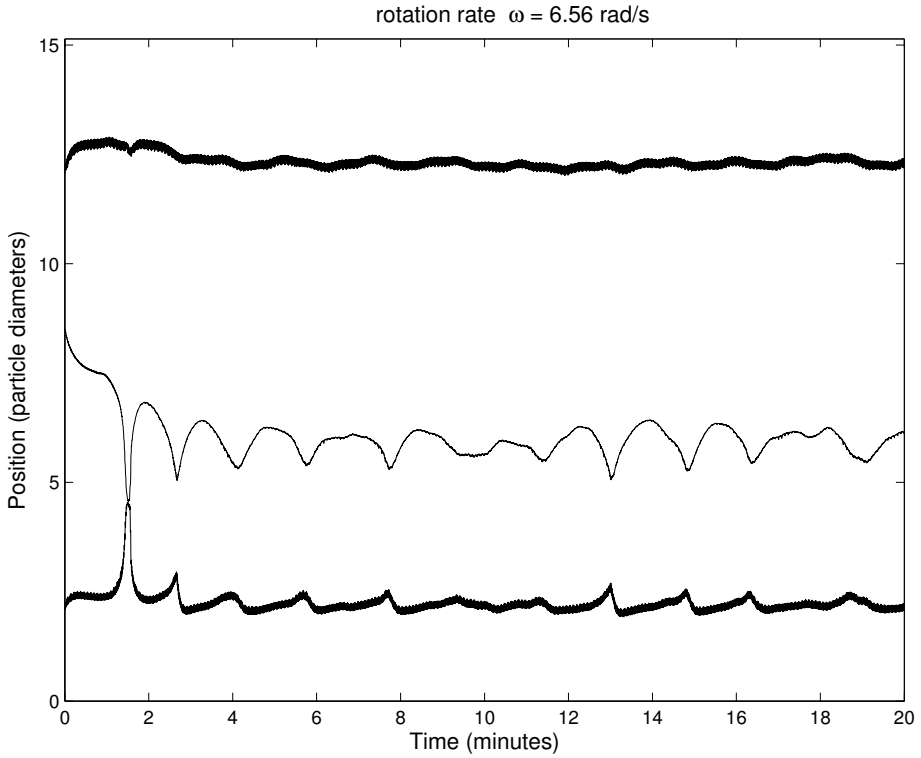

Figure 4.5: The biased chaotic state is the first of two types of chaotic behavior seen in the experiment. In this case, the center bead will favor collisions with one of the outer beads exclusively. Much like the doublet state, the choice of which outer bead to favor is seemingly dependent on initial conditions.

For higher ω chaotic states, the beads explore a more rich set of interactions, including pair collisions (left-middle and right-middle) as well as triplet-type collisions where all three beads come together. Figure 4.6 shows a typical example of this behavior, which we call the fully chaotic state. In pair collisions, beads can be either in phase or out of phase with one another. In phase collisions are more direct, with the beads immediately colliding and moving away, while out of phase collisions often involve the beads cascading over one another several times before colliding. Triplet-type collisions generally involve two beads cascading over one another while a third bead approaches and collides with them.

Already, with the description of these states, we have observed some previously unseen behavior. Specifically, the doublet and triplet states have not been described in previous drum rotation work [18]. The doublet state can be thought of as an analogous state to the long-term behavior seen in the Jánosi simulations [13], where two beads pair up and leave the third behind, but there is no similar analogue for the triplet state. Furthermore, the distinction between biased and full chaotic states has not been previously described.

4.2.2 Phase Diagram

In order to probe the dependence of the particles' behavior on rotation rate, we recorded sixty-eight videos at rotation rates ranging from 5.1 to 12.3 radians per second. An analysis of these videos allowed us to map out a phase diagram as shown in Fig. 4.7.

This phase diagram has several interesting regimes, denoted by various color blocks in the phase diagram. Gray blocks represent regimes where there is some overlap of behavior, or transitions between two regimes. The width of these transition blocks is due to uncertainty both due to the measurements themselves, and also to the discrete,

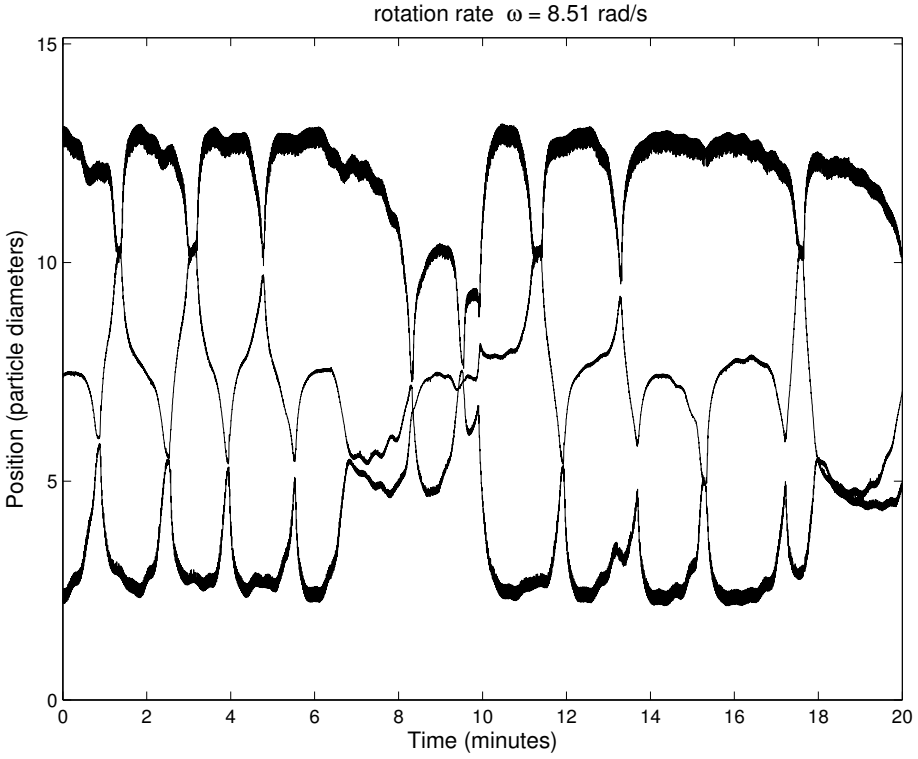

Figure 4.6: The fully chaotic state of the system is a state in which there is no apparent bias toward either of the outer beads, and all three beads interact chaotically with a variety of different collision types. Collisions of two particles sometimes involve two beads that are in-phase in the cascade motion, so the beads have similar y values, leading to a direct collision in the x direction. Alternatively, two-particle collisions can involve beads that are out of phase, such that the particles cascade on top of one another in a motion similar to the doublet phase for a few rotations before colliding and splitting apart Three-particle collisions usually involve two beads in a doublet-like configuration coming close to the third bead, either in-phase or out of phase.

digital motor control circuit, which limits the resolution of ω. Symbols below these blocks indicate individual measurements. Labeled points above the blocks indicate measurements which were used for example plots elsewhere in this Dissertation.

With increasing rotation rate ω, the system undergoes a phase transition from periodic to biased chaotic behavior, which is then followed by a long doublet regime. After this doublet regime, we find a small window of triplet behavior around $\omega \sim 7.8$ rad/s.

At rotation rates slightly beyond this triplet window ($\omega \sim 7.9 - 8.4$), we find a curious mixed regime, where it is difficult to describe the exact behaviors found. Within this range of rotation rates, some measurements appear to indicate a chaotic behavior, while others imply triplet behavior. Perhaps more remarkably, separate measurements at the same rotation rate can give conflicting results, with some indicating triplet and others chaotic behavior. A possible explanation for this result is presented in Sec. 4.2.3.

Beyond the triplet phase lies a regime of reliably chaotic behavior, split by a small window of repeatable triplet behavior in the middle. This chaotic regime is followed by a longer window of triplet behavior for $\omega \sim 9.5 - 10.4$, with a single measurement within this regime indicating a chaotic trajectory. This could again be a result of long transients as discussed in Sec 4.2.3.

For rotation rates higher than those at which we find triplet behavior, we find reliable doublet trajectories, until, for high enough rotation rates, we transition into solid-body rotation as described by Mullin [18]. This regime is not represented in our measurements due to limitations in the apparatus discussed in Sec. 3.1.1.

This phase diagram illustrates a rich landscape of interesting regimes of particle behavior with a new level of detail. Specifically, previous work identified only one simple, contiguous block of chaotic behavior [18], while we have identified multiple windows of periodic behavior embedded within large chaotic regimes, as well as pre-

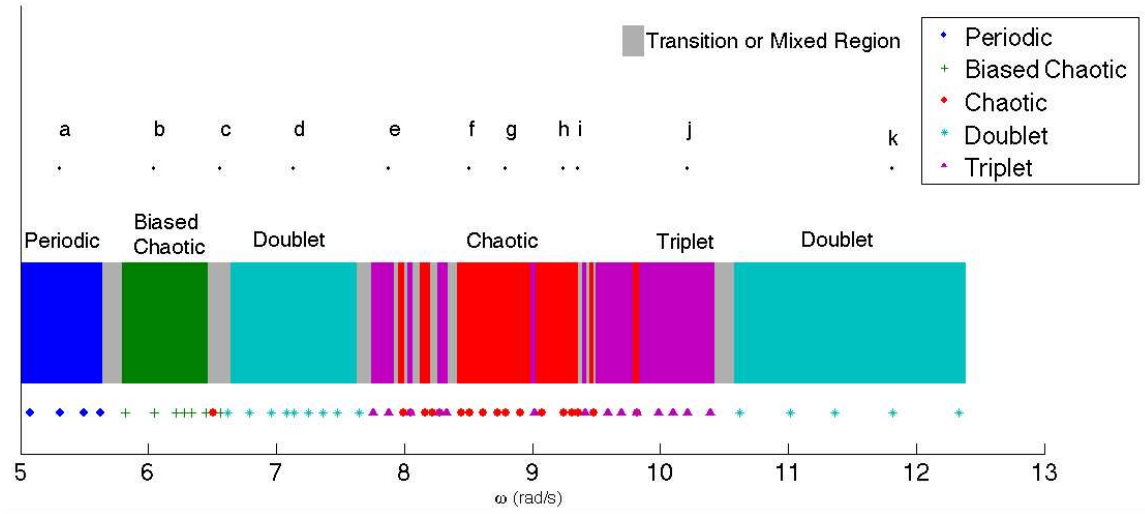

Figure 4.7: The system exhibits a variety of behaviors at various rotation rates. At the lowest and highest rates, predictable steady-state behavior occurs, but at intermediate rotation rates, a mix of both chaotic and steady-state behaviors can be found.

Labeled points at the top of the graph show where the various example figures within this paper are located on the phase diagram.
(a) Fig. 4.2 (d) Fig. 4.3 (e) Fig. 4.4 (c) Fig. 4.5 (f) Figs. 4.6, 4.10 (g) Figs. 4.12, 4.13, 4.14 (a,b,h,i,j,k) Fig. 4.15

viously unidentified periodic behaviors. Furthermore, the distinction between two different types of chaotic behavior illustrates the depth and complexity of the system.

4.2.3 Transients and Motor Stability

There are two inter-related caveats to be considered when discussing the phase diagram in Fig 4.7. The first of these is the issue of transient behavior. In a given experiment, after the drum begins rotating, the system takes some time to settle into its long-term behavior. For example, in Fig. 4.4, the particles move back and forth across the drum, colliding several times before finally coming together to form the triplet state at $T \sim 12$ min. In this case, the time is small compared to typical experimental durations ($T \sim 300$ min). However, in other experiments, such as that shown in Fig. 4.8, transient behavior can persist for longer periods of time. Here, the trajectory is seemingly chaotic for ~ 120 min before settling into a stable triplet configuration.

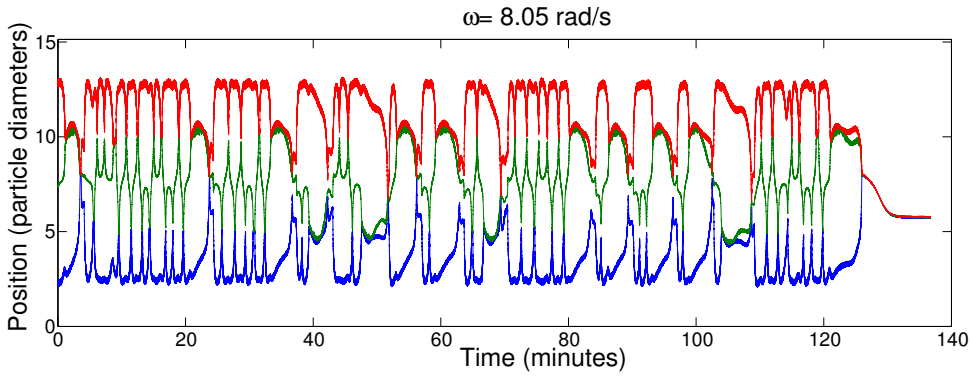

Figure 4.8: In this experiment, the particle follows a seemingly chaotic trajectory for ~ 120 min, but then settles into a stable triplet state.

In order to further explore the impact of these long transient trajectories, we examine each trajectory by eye, and manually determine an approximate transient duration. Figure 4.9 shows this transient duration plotted versus the rotation rate of

the drum. The symbols in the graph represent the type of trajectory found after the transient behavior has died out.

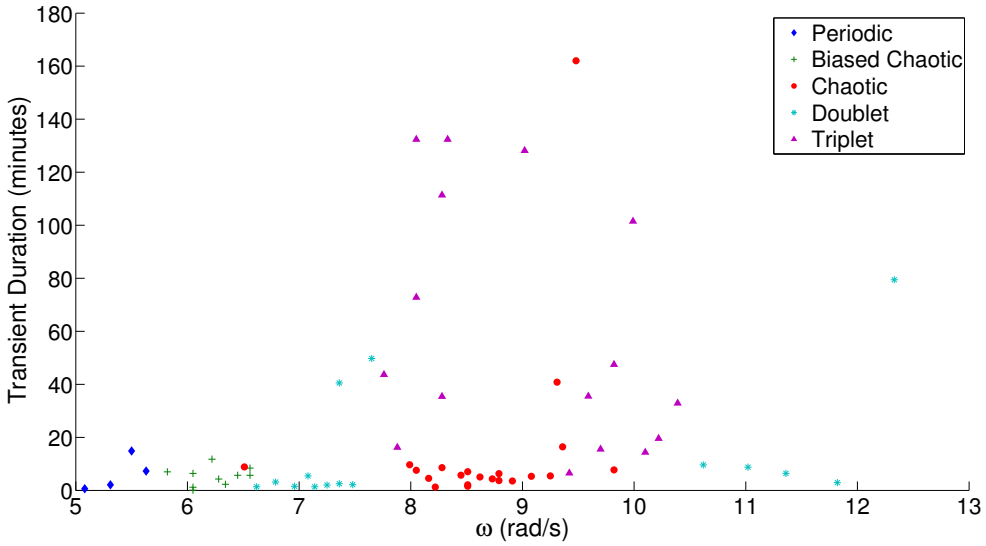

Figure 4.9: After the motor is started, it typically takes some amount of time for the system to settle into its long-term behavior. The approximate time taken for the initial transient behavior to die out is obtained by eye and plotted versus rotation rate. Symbols represent the long-term phase of each trajectory, after its transients have died out.

We note that the bulk of trajectories seem to have relatively short transient times, with transients rarely exceeding sixty minutes in duration, or roughly one sixth the duration of a typical measurement. However, there are also trajectories which contain much longer transient durations, with most of these long-duration transient trajectories clustered around the transitions between different phases. We consider two possible explanations for this behavior.

In Sec. 3.1.1, we noted that drum rotation rates are stable to within $\sim 1\%$. If we consider the transition around $\omega = 8$ rad/s, we see that, for a given trajectory, ω could vary from 7.92 to 8.08 rad/s, significantly blurring the transition region. We propose that a possible source for the presense of these long transient behaviors is drift in rotation rate of the drum motor. If we imagine small windows of triplet behavior within a chaotic regime, a drum rotation rate which starts within the chaotic regime

could drift into the triplet regime, leading to a trajectory which eventually "finds" the triplet state. As already discussed, the triplet state is very robust and stable, and thus once a trajectory finds this state, it would be very difficult to break out of it, even if the rotation rate did wander. The fact that long transients tend to cluster around the transitions between regimes lends some credibility to this hypothesis.

This issue of motor drift also has the potential to obscure some detail in the phase diagram. The motor control has finite resolution in available rotation rates, and so there may be small windows of behavior which we are unable to locate. Similarly, even if we did sample these windows, motor drift could take the rotation rate out of a window if it existed within a very narrow range of rotation rates.

A second possibility is that the trajectories simply have some varying transient period, and our samples are only able to capture those whose transients lie within the time frame of our experiment. Triplet states, in particular, are very stable, and once a given trajectory manages to find one of those states, it is unlikely to escape. Thus, there is potential for many chaotic states to be triplet states in reality. However, some rotation rates never find even triplet-like behavior in their collisions, so those states would be likely remain persistently chaotic. In order to test this, it would be necessary to re-design the apparatus in order to increase the stability of the rotation rate to rule out drift. This would be a worthwhile endeavour, and deserves further attention in the future.

4.3 Qualitative Fluid Behavior

In order to qualitatively describe the fluid flow within the drum, we added a small quantity of Kalliroscope rheological fluid to the glycerol within the drum. Kalliroscope is a water-based suspension of microscopic crystalline platelets. When placed within a moving fluid, the platelets tend to align such that their long axis is parallel to the

plane of shear. Thus, the platelets will reflect different amounts of ambient light depending on the local flow of the fluid. This allows us to visualize the flow behavior in each of the states, as described below.

4.3.1 Periodic Regime

Within the periodic regime, the three beads each has a well defined wake, which is bounded on each side by swirling, vortex-like behavior rotating about an axis that extends in the radial direction. At the mid points between each pair of particles, there are well defined shear planes which span the entire height of the drum. These shear planes are continuous sheets in the $y - z$ plane in which all of the Kalliroscope is aligned in the same direction, corresponding to a region where there is a strongly sheared boundary between two distinct flows.

4.3.2 Doublet Regime

In the doublet regime, the two beads which are paired up form a wake which keeps them aligned with one another. This wake is bounded on each side by vortex-like regions where there is swirling fluid flow. The single bead, well-separated near the far end of the drum, also has a well defined wake, but there is significantly less vortex-like behavior in the fluid. At an intermediate point between the single bead and the pair of beads, there is a well defined shear plane that spans the entire height of the drum, and oscillates slightly in position in phase with the cascade of the single bead.

4.3.3 Triplet Regime

In the triplet regime, there is one strong wake in which all three beads cascade. There is a large amount of vortex-like swirling that bounds this wake and likely leads to the observed stability of the triplet state.

4.3.4 Biased Chaotic Regime

The flow within the biased chaotic regime appears similar to that within the periodic regime, except when the beads collide. As the beads approach a collision, their wakes overlap and partially merge. At the same time, as the beads are approaching one another, the shear band that separates them oscillates with greater and greater amplitude, until it breaks up as they approach. After a collision, when the beads are moving apart, the fluid to the outside undergoes a strong vortex-like swirling until the beads are well separated.

4.3.5 Fully Chaotic Regime

Within the fully chaotic regime, the beads' wakes are often less well defined and more difficult to identify, with large regions of complicated fluid flow. However, when the beads are well separated, their wakes are evident, with the wakes becoming mixed and obscured as the beads approach one another. The well defined shear planes seen separating the beads in previous cases are not evident in the fully chaotic regime.

4.4 Fourier Analysis

A visual inspection of representative chaotic trajectories seems to indicate a typical time between collisions of the particles. For example, if we look more closely at Fig. 4.6, many of the collisions between particles occur roughly 1-2 minutes apart. In order to study this in more detail, we applied a discrete Fourier transform to each of the trajectories, as given in Eqn. 4.1.

$$X(k) = \sum_{j=1}^{N} x(j)\omega_N^{(j-1)(k-1)}, \tag{4.1}$$

where $\omega_N = e^{(-2\pi i)/N}$.

In order to find the most prevalent frequencies for a given trajectory, we plot the spectral density $\Phi(f) = X(f)X^*(f)$ as a function of frequency f (cycles per minute). We do this for each of the three particles within a given experiment, as shown in Fig. 4.10, on both semi-log and linear plots. On these example plots, all three particles show a large peak at a frequency of approximately 0.8 cycles per minute. This agrees well with visual inspection of the trajectories, where typical times between collisions are on the order of $1 - 1.5$ seconds. Thus, the largest peak in the Fourier spectrum serves as a measure of the dominant period of the particle collisions. We find that, for a given rotation rate, these spectra are often, but not always reproducible. However, similar rotation rates will often have similar spectra. This leads us to conclude that the occasional lack of reproducibility could be attributed to motor drift as discussed in Sec. 4.2.3. This also makes it difficult to draw conclusions from the smaller peaks in the Fourier spectra, as they are less reproducible than the main peaks.

In Fig. 4.11 we calculate these three spectra for every experiment, and plot the frequency corresponding to the maximum spectral density for each rotation rate. For biased chaotic trajectories, we swap x_1 and x_3 as necessary to ensure that x_1 is always the trajectory of the bead which is interacting with the center bead. Figure 4.11 gives a basic understanding of how the dominant period of the trajectories changes with rotation rate.

For the doublet regime, we surprisingly see some measurements with periodic motion in the horizontal direction. This corresponds to doublet behavior where the two beads are cascading slightly off-center from one another, so that they oscillate back and forth in the horizontal direction.

For the biased chaotic regime, there seems to be little variation in the periodicity for various rotation rates, at least in the x_1 and x_2 measurements, which indicate the two beads which are interacting. Any periodic behavior that would be seen in x_3 would tend to be smaller in amplitude, due to its isolation, and thus there is more

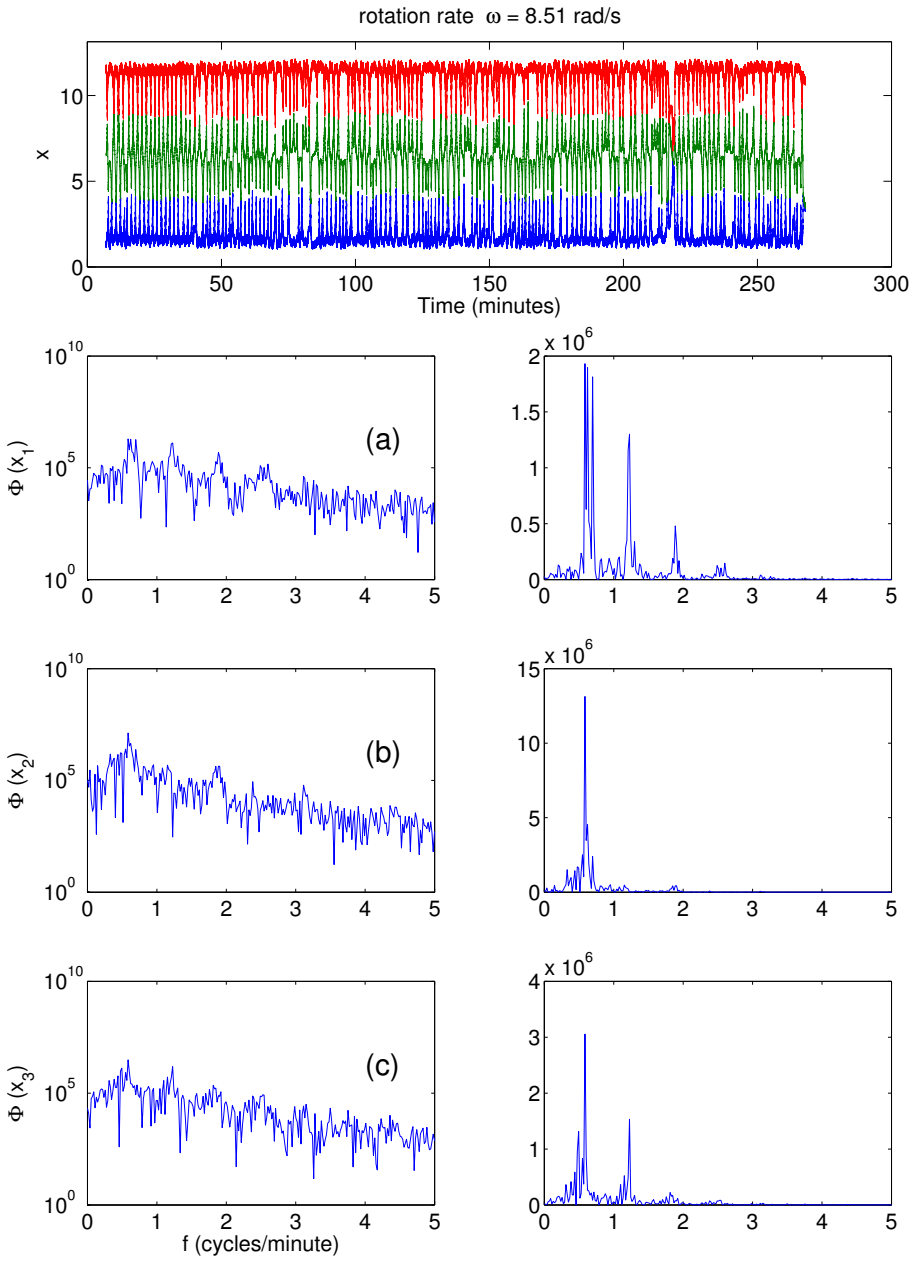

Figure 4.10: Spectral density is plotted versus frequency for each of the three beads in an example chaotic time series. In the left column, frequency is plotted on a log scale, while the right column frequency scale is linear. Particle (a) corresponds to the blue trajectory, (b) to green, and (c) to red. Notice that the largest peak in each case occurs at a frequency of approximately 0.8 cycles per minute, corresponding to a period of 1.25 minutes between collisions. This is in agreement with visual inspection of the trajectories.

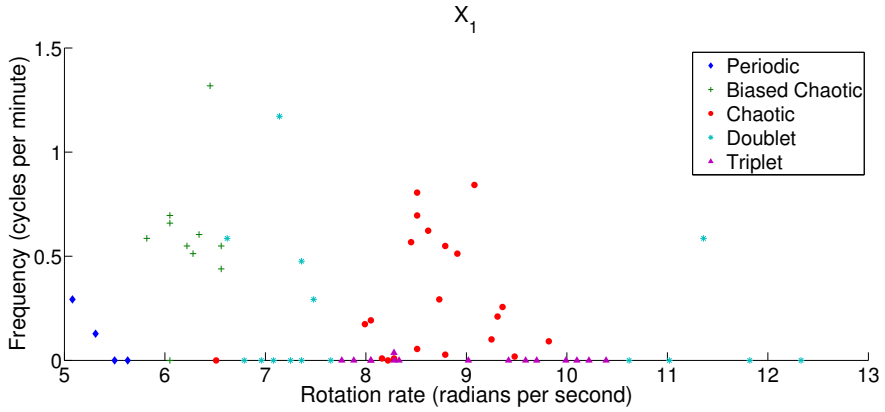

(a)

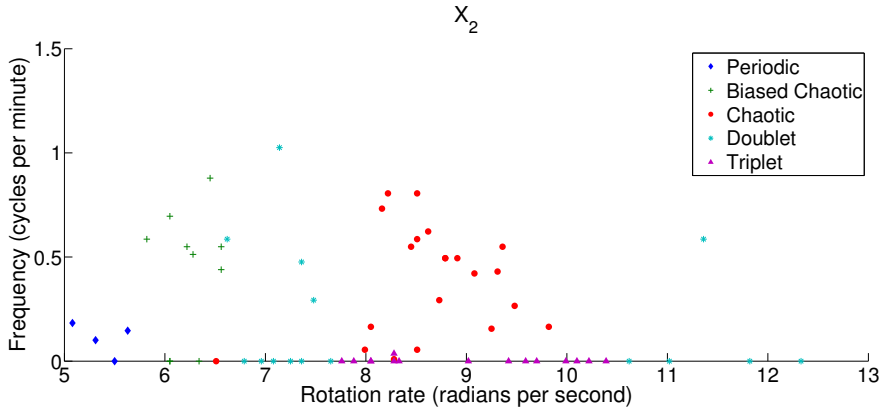

(b)

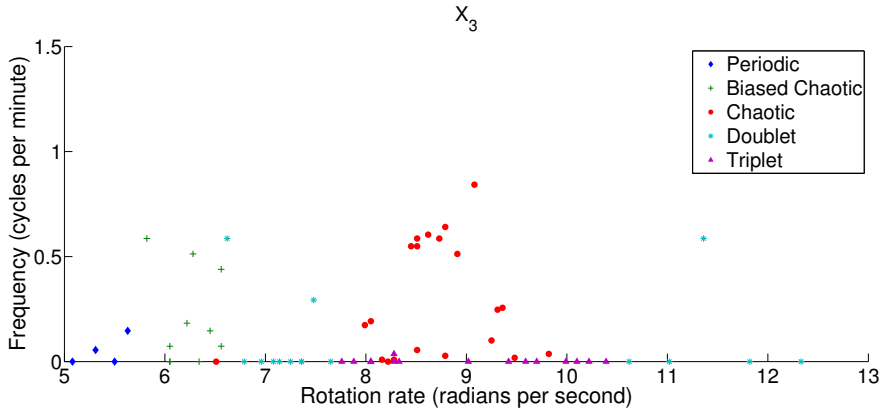

(c)

Figure 4.11: The frequency corresponding to the largest spectral density value is plotted versus rotation rate for the trajectory of each of the three beads. Note that the graphs for the outer beads have similar shapes, however in those situations where there is a bias, x_1 always represents the biased side, while x_3 is the isolated particle.

scatter in the x_3 measurements.

Within the full chaotic regime, the peak frequencies are far more scattered. The least scattered of the three measurements is that of the center bead, x_1, with a large number of points implying a linear relation between frequency and rotation rate, with negative slope. The few outliers which deviate from this linear behavior may represent transient chaotic trajectories which were unable to reach their final periodic state within the time frame of the measurement.

Triplet and many doublet trajectories tend to have their peaks at $f = 0$, corresponding to a trajectory lacking periodic behavior in the x direction, as expected for these non-chaotic motions. The underlying periodic cascade in the $y - z$ plane, due to drum rotation, will not show up in this x plot.

This Fourier analysis provides a measurable quantity which serves as an indicator of periodic behavior within various regimes. Non-chaotic regimes, for the most part, show a lack of periodic motion in the horizontal direction, while still exhibiting the periodic cascade in the $y - z$ plane exhibited by all cascade regimes. Chaotic regimes demonstrate two types of behavior, a constant dominant frequency for biased chaotic trajectories, and a dominant frequency that decreases linearly with rotation rate for chaotic regimes. Outliers within the chaotic regime may serve as an indicator of potentially transient chaotic behavior with duration longer than our measurement time.

4.5 Reduced Dimensionality Analysis

4.5.1 Reduced Dimensionality

To this point, all analysis has focused on the horizontal (x) direction trajectories, and neglected cascading in the $y - z$ plane. In order to further simplify the number of variables used in the data analysis, we sought a reduced dimensionality set of

variables which still contains the interesting behavior of the system. We note that, once trajectories have settled into their long-term behaviors, and the transients have died out, the center of mass of the system is nearly constant over time, as shown for an example trajectory in Fig. 4.12.

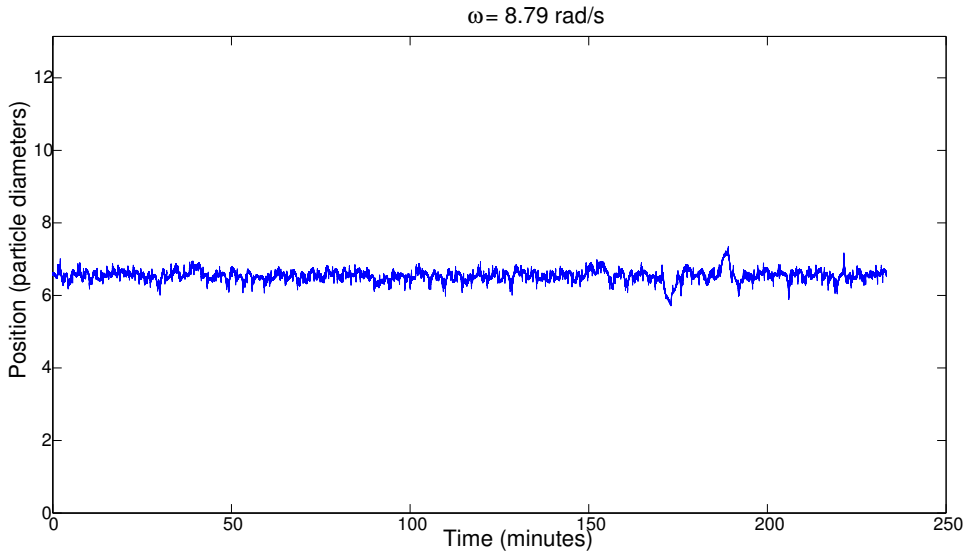

Figure 4.12: The position of the center of mass, $x_{com} = (x_1 + x_2 + x_3)/3$, is plotted versus time for a typical chaotic trajectory. Note that the position of the center of mass is nearly constant with time.

This implies that the absolute positions of the particles are not needed to capture the interesting behavior of the system, and we can use a reduced dimensionality to study the behavior. Specifically we use the distances of each outer bead from the center bead:

$$x_{21} = x_2 - x_1 \tag{4.2}$$

$$x_{31} = x_3 - x_2 \tag{4.3}$$

with the order chosen in this way so that the results will always be positive. Figure 4.13 shows a sample of the same trajectory with this reduced dimensionality data

set plotted versus time.

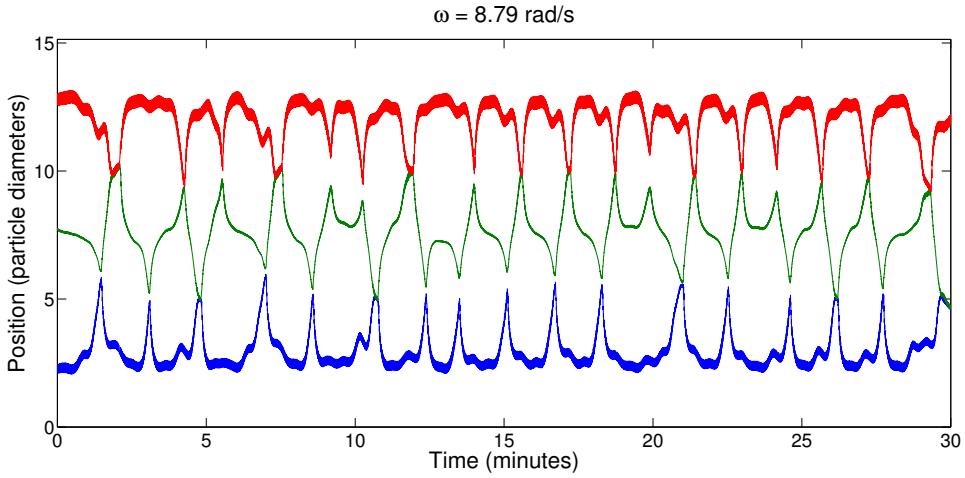

(a) Original three particle trajectories

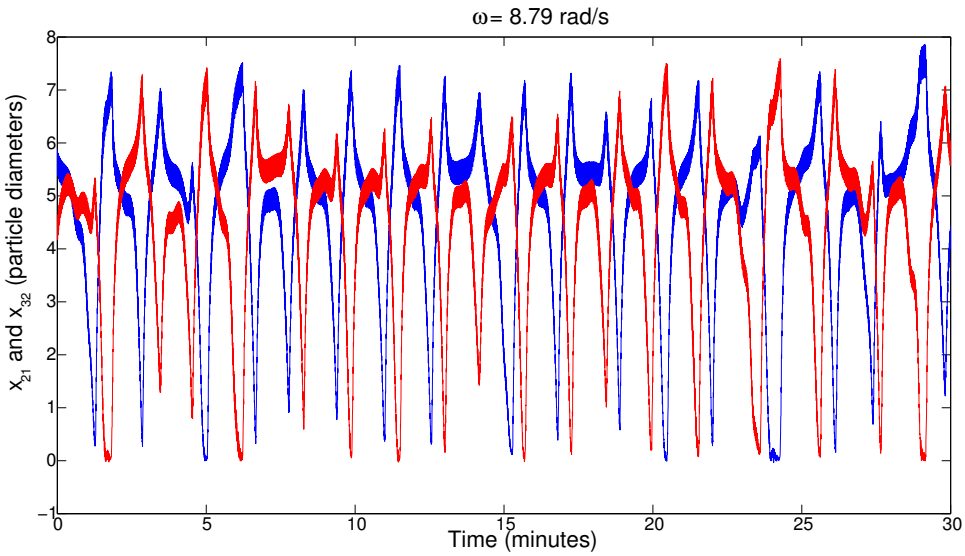

(b) Reduced dimensionality trajectories

Figure 4.13: The original particle trajectories (a) can be simplified to give a reduced dimensionality phase space (b). The simplified trajectories, including only x_{21} and x_{32}, still capture all of the interesting collision behavior of the system.

4.5.2 2-D Histograms

An interesting question is posed by the consideration of which configurations the system spends the most time in. In other words, is most of the time spent with the

three beads spread evenly apart, or is more time spent with some combination of the beads close together? To study this, we plot a two dimensional histogram of the configurations, which gives us a way to visualize the relative amount of time each particle spends in various regions of phase space.

In each experiment, we visually inspect the data set and remove any obvious initial transient behavior manually before analysis. So, for example, the analysis of a triple data set only includes the time after the three beads have paired up.

Figure 4.14 shows an example of one of these histograms, again for the same experiment used previously in this Section. Notice that the darkest red region is in the area around $x_{21} \sim 5-6$ and $x_{32} \sim 5-6$, corresponding to a configuration where the three beads are spread far apart, and spaced roughly equidistantly. There are also small clusters at $x_{21} \sim 7.5$ and $x_{32} \sim 0$, and its mirror $x_{21} \sim 0$ and $x_{32} \sim 7.5$, which correspond to configurations where two beads are close together, and the third bead is far away. Finally, there is another faint cluster at $x_{21} \sim 0$ and $x_{32} \sim 0$, corresponding to a state where all three beads are grouped together. The faintness of this cluster implies that very little time is spent in this configuration.

If we look at these histograms for trajectories at various rotation rates, we can visualize how different phases of the system explore phase space. Figure 4.15a shows the histogram for a periodic trajectory, with the three beads spaced roughly equidistantly. The slight amount of smearing corresponds to a faint periodic oscillation in the x direction. In Fig. 4.15b, the histogram for the doublet state shows two beads clustered close together in phase space, with the third separated by some distance. Similarly, Fig 4.15c shows all three beads clustered together. Figure. 4.15d shows a biased chaotic trajectory, where the beads spend some time in the same region of phase space as the periodic state, but also wander chaotically in the x direction, smearing the histogram in the direction of the bias. In Fig. 4.15e we see a more complicated chaotic trajectory, with a variety of interactions represented. The beads

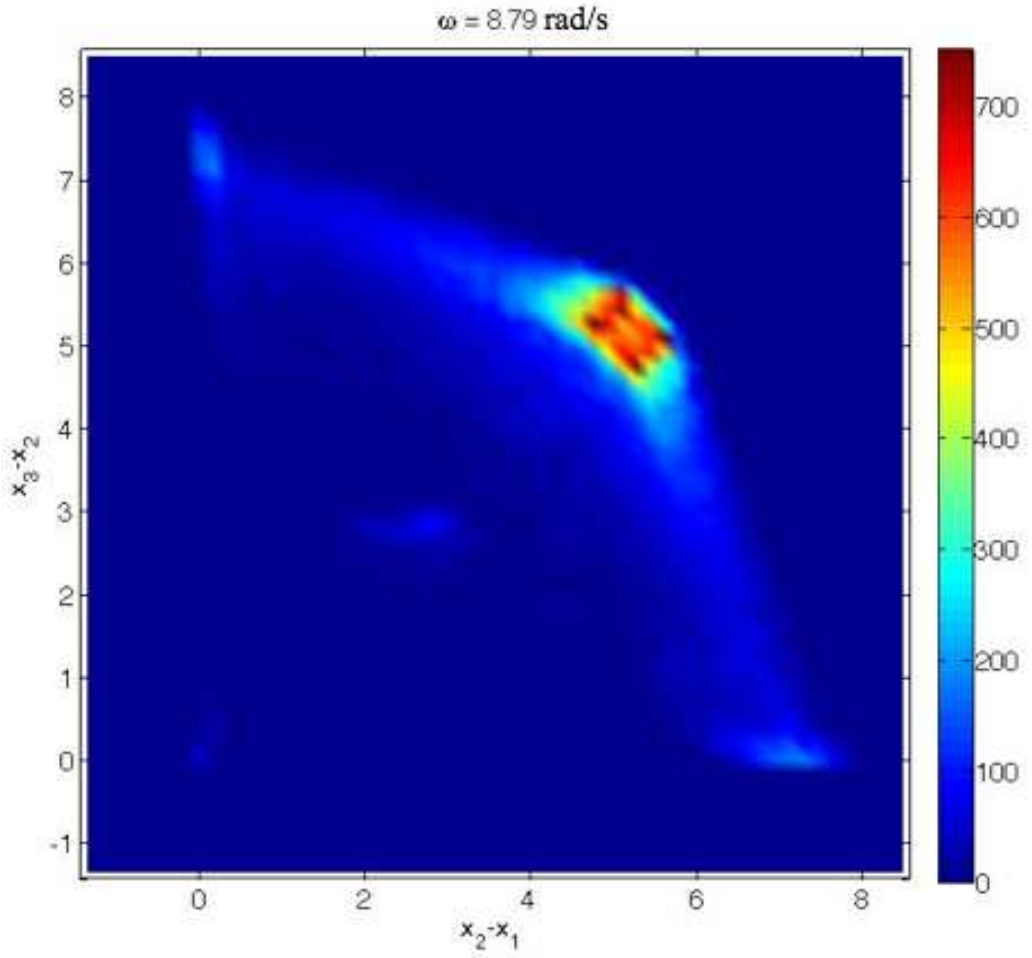

Figure 4.14: A typical two dimensional histogram for a chaotic trajectory. The axes represent the distances between the pairs of particles, normalized by the particle diameter, and color represents the number of points that were counted in each bin. Red indicates that the system spent a significant amount of time in that configuration, while blue indicates that the system spent little time there. This trajectory has a calculated entropy $S = 6.33$.

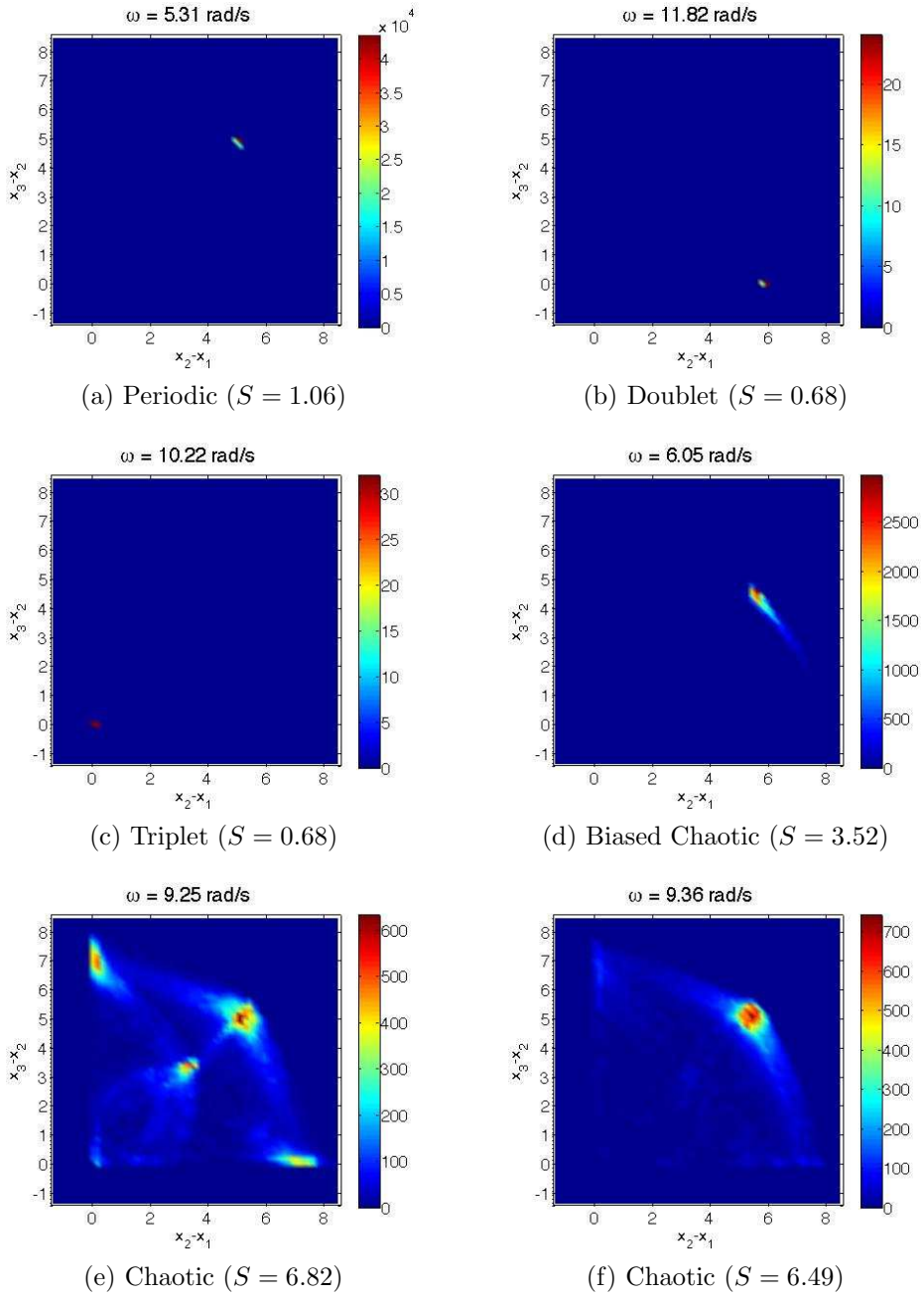

(a) Periodic ($S = 1.06$)

(b) Doublet ($S = 0.68$)

(c) Triplet ($S = 0.68$)

(d) Biased Chaotic ($S = 3.52$)

(e) Chaotic ($S = 6.82$)

(f) Chaotic ($S = 6.49$)

Figure 4.15: Histograms for each phase of behavior clearly illustrate the amount of phase space they explore. Histograms for periodic trajectories (a) show the three beads spaced evenly apart, and never wandering from a small region of phase space. Histograms for doublet (b) trajectories show two beads with nearly the same x position, and the third separated by a large distance, while those for triplet states (c) show all three beads with little or no spacing between them. Biased chaotic trajectories include the same region of phase space as a periodic trajectory, with an additional "smearing" which shows two of the beads coming closer together as they wander chaotically in the x direction. Chaotic trajectories (e,f) show more complicated behavior, with more of phase space explored by the system.

explore the phase space around triplet and doublet states, as well those seen in periodic trajectories, and another intermediate configuration where the three beads are closer together than in the periodic trajectory, but not clustered like in the triplet state. This is in contrast to Fig. 4.15f, where the beads spend the bulk of their time well-separated, as in the periodic state, with occasional collisions. The fact that these states occur at rotation rates which are very similar ($\omega = 9.25, 9.36$ rad/s) illustrates how sensitive the experiment can be to rotation rate.

These histograms give us a powerful way to visualize the way in which a given experiment explores phase space as discussed in Sec. 1.3. Periodic behaviors tend to explore very few of the possible configurations of particles, leading to mostly blue histograms with a small dark red region representing the small region of phase space occupied by the trajectory. Chaotic trajectories, on the other hand, explore more of phase space, and this is borne out in the histograms, with biased chaotic trajectories exploring fewer configurations than the more thoroughly mixing full chaotic state. Completely abstracting away the exact details of the particle motion, these diagrams of phase space exploration indicate particle behavior at a glance.

4.5.3 Entropy

To quantitatively study the extent to which a given trajectory explores phase space, we define a configurational entropy based on these histograms. If we first normalize a given histogram so that the sum of all bin values is equal to unity, the histogram will represent a probability distribution P with matrix elements P_{ij}. We then define the entropy

$$S = -k \sum_{ij} P_{ij} \log P_{ij} \quad , \quad \text{with } k \equiv 1. \tag{4.4}$$

This entropy value is calculated for each individual trajectory and plotted versus rotation rate in Fig. 4.16. Note that, for typical chaotic rotation rates, the entropies

tend to be higher, while for periodic, doublet, and triplet states, entropies are lower, as expected. Furthermore, the full chaotic states have larger entropies than biased chaotic trajectories.

We explore two possible methods to quantify the error in these entropy measurements. The first is the propagation of statistical error in the number of counts in each bin. Thus, the error in the probability of a given bin is $\Delta P_{ij} = \sqrt{N_{ij}}/N$, where N is the total number of counts, and N_{ij} is the number of counts in the i,jth bin. If we propagate the error in each probability measurement, we find that the error in entropy is:

$$\Delta S = \sqrt{\sum_{ij}([1 + \log P_{ij}]\Delta P_{ij})^2} \tag{4.5}$$

The second method to quantify error in entropy measurements is to split each trajectory into two halves, and calculate the entropies S_1 and S_2 for each half independently. Then the error can by defined as:

$$\Delta S = |S_1 - S_2| \tag{4.6}$$

Of these two, the second method is consistently an order of magnitude greater than the first, so we chose to use the two halves error estimation technique to quantify our error, as shown in Fig. 4.16.

At the lowest rotation rates, where behavior is periodic, entropy is small, as expected, as the particles explore very little of phase space. As this periodic regime transitions into the biased chaotic regime, there is a sudden jump in entropy, demonstrating the sharp transition from periodic behavior to behavior in which particles begin to wander in the horizontal direction. Within the biased chaotic regime, entropy decreases with increasing rotation rate until it transitions into a doublet regime. At that transition, there is another sharp jump, this time to low entropy. This entropy increases slightly with rotation rate within the doublet regime until the jump

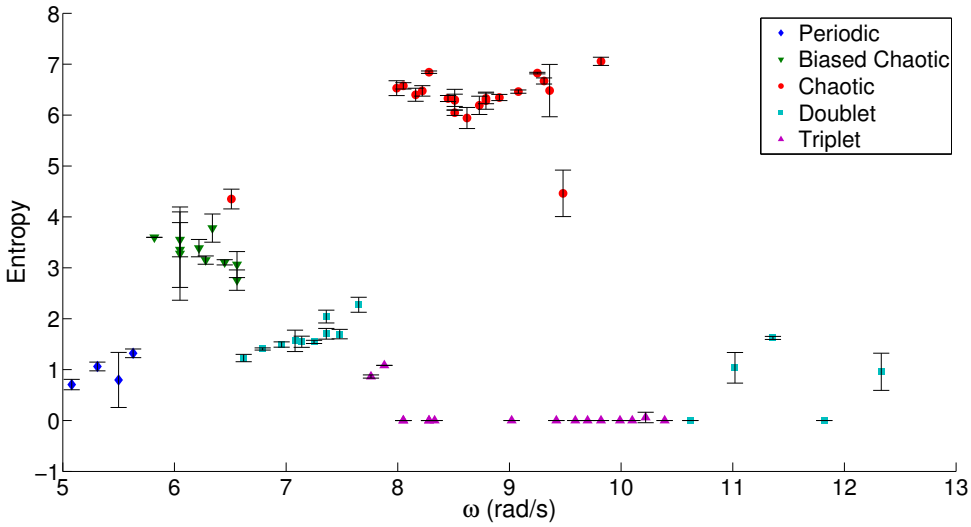

Figure 4.16: This figure shows the entropy for each rotation rate, calculated from the 2-D histograms.

to the large entropies of the full chaotic behavior, with a mix of low-entropy triplet behavior within the large block of chaotic behavior. Finally, there is another jump to low-entropy behavior within the large ω triplet and then doublet regimes.

Much as the histograms provide a visual indication of the degree to which a trajectory explores phase space, these entropy values provide a qualitative measure of that exploration. Low entropy periodic, triplet, and doublet regimes do not explore phase space much, as expected. Chaotic behaviors, on the other hand, have large entropies, corresponding to strong mixing and indicative of chaotic behavior. Despite the large variations in entropy when transitioning from one regime to another, within each block of chaotic behavior, the entropies vary little by comparison, indicating that the amount of phase space explored by chaotic behaviors does not vary much with rotation rate within each chaotic regime. For the biased chaotic regime, the amount of phase space explored decreased with increasing rotation rate until the particles are able to lock into a doublet state, indicating an evolution of the biased chaotic states with increasing ω. The full chaotic regime, by contrast, has more scattered entropy, with no obvious trend with ω. This, along with the scattering of triplet states within

the chaotic regime, implies that behavior within this regime is more complicated than a simple linear ω dependence as we saw within the biased chaotic regime.

4.5.4 Bin Sizes

To this point, we have neglected the influence of the size of bins on the entropy measurements. If we consider a single bin which spans the entire configuration space, $P = 1$, and $S = 1\log 1 = 0$. At the other extreme, if the size of the bins tends toward zero, the number of counts in any one bin will be either 0 or 1, so if the total number of counts is N, the probability of any one bin being occupied will be either $P = 0$ or $P = 1/N$, resulting in an entropy $S = -\log(1/N) = \log(N)$.

In between these two extremes, calculated entropy values will vary with the bin size. For example, in Fig. 4.17 we see that the entropies for each rotation rate are shifted for histograms consisting of 180^2 bins compared to those calculated for 60^2 bins. The trends in entropy behavior, however, remain the same for both examples.

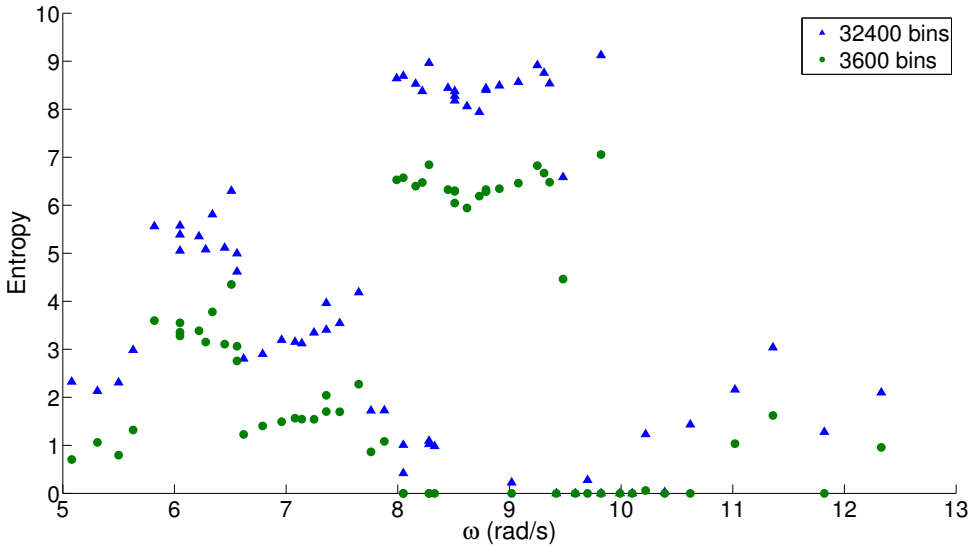

Figure 4.17: This figure shows the entropy for each rotation rate, calculated from the 2-D histograms, with histograms consisting of two different bin sizes, corresponding to a total of 180^2 or 60^2 bins.

Studying these variations in entropy values, we attempted multiple scaling tech-

niques to try to identify a preferable bin size, and were unable to do so. We chose to divide each axis into 60 divisions, giving a total of 60^2 bins. This value was chosen by looking at graphs of entropy versus bin size rate for several example trajectories, and noting that the trend in entropies within the regime around $40^2 - 80^2$ bins looked well-behaved and linear. You could certainly illustrate the same trends with other choices for bin size, but consistently using 60^2 bins allows us to compare our entropies between various trajectories and identify trends.

4.6 Variation of Parameters

In this work, we have studied the behavior of the rotating drum as the rotation rate is varied over a wide range. There are many other parameters which could change the behavior of the system. Below we discuss conjectures for how slight perturbations of several parameters might affect the behavior, although these conjectures have not been confirmed by experiments.

Viscosity Decrease

With a decrease in the viscosity, we would expect the strength of the interactions between the particles to weaken. This decrease in the strength of interactions would tend to make the periodic regime span a larger range of rotation rates, as the cascade amplitude would need to be larger for the beads to begin interacting. At the large rotation rate regime, we would not expect the transition toward solid body behavior to move, as the influence of centrifugal force compared to gravity would not change. At moderate rotation rates, we would expect the chaotic regime to shrink, and doublet regimes to expand, as the lower interaction strength would make it more difficult for the beads to be drawn back together once they separated into a doublet-like configuration. We would expect the peak frequency values to be shifted in the direction of

larger frequencies, as the lower viscosity would correspond to faster-moving particles. Entropy values would tend to decrease slightly, as the strength of the interactions, which drive the exploration of phase space, would weaken.

Length Scale Decrease

If we imagine scaling all lengths within the cylinder downward slightly, the bead radius, drum radius, and drum length would all decrease. In this case, both the characteristic velocity $U = \omega r_c$ and the characteristic length scale r_b would decrease, leading to a smaller Reynolds number $Re = UL/\nu$. This would effectively be equivalent to an increase in viscosity, with all trends being the opposite of what is seen if viscosity is decreased.

Decrease in Gravitational Force

If the external gravitational force on the beads is decreased, we expect similar results to the viscosity decrease. Decreasing the strength with which the beads are pulled through the fluid would would decrease the strength of their interactions, leading to the same trend as in the viscosity decrease, with one exception. Since the strength of gravitational force is decreased, but centrifugal force remains the same, we would expect the transition to solid body rotation to be shifted to the left, to lower ω. As we already discussed, the decrease in interaction strength would shift the transition away from periodic motion to the right, to larger ω. These two effects combined would tend to make the middle region of the phase diagram narrower.

Chapter 5

Summary and Outlook

5.1 Summary

In the measurements and analysis performed in this Dissertation, we have demonstrated a geometrically simple system containing three particles moving within a fluid-filled rotating drum which yields a rich and varied set of behaviors. The phase diagram for this system showed five types of behavior. The first is a periodic regime where the beads simply cascade in the $y - z$ plane. The second is a previously unreported biased chaotic regime where two of the beads wander chaotically in the horizontal x direction and collide with one another. The third is a doublet regime, where two beads pair up and cascade on top of one another while leaving the third bead behind. There is also is a mixed chaotic regime spanning a wide range of rotation rates, where the beads wander chaotically in the horizontal direction, with all three beads interacting and mixing. Within this mixed regime, there are small windows of rotation rates which result in triplet behavior, where all three beads will line up and cascade on top of one another. Finally, we find a regime where triplet behavior is the only type of trajectory seen.

In order to both qualitatively and quantitatively study these various behaviors, we looked at two main analysis techniques, neither of which have been applied to this

geometry before. The first of these was Fourier analysis, which allowed us to identify the dominant frequency within the horizontal motion of a particle. For the most part, periodic, doublet, and triplet trajectories showed no dominant frequency, as expected, due to their lack of motion in the x direction. However, a few doublet states were found to exist where the two cascading beads were not directly in line with one another, and thus oscillated periodically in the horizontal direction. Biased chaotic trajectories showed a well defined dominant frequency, corresponding to the typical collision time of the particles. This frequency value was approximately constant, with a value around 0.6 cycles per minute. Pure chaotic trajectories also showed a well defined typical collision frequency, but their values decreased linearly with increasing rotation rate.

The second analysis technique involved abstracting away the exact particle positions to study the nature of the collisions. A two-dimensional phase space, consisting of the distances between pairs of particles, was constructed and used to create histograms. These histograms provided a visual representation of the degree to which each trajectory explores phase space, with periodic, doublet, and triplet states exploring very little phase space, while biased chaotic and full chaotic states explored much more of phase space, corresponding to an increase in topological mixing.

By defining an entropy value based on these histograms, we were able to qualitatively measure the extent to which a given trajectory explored phase space, and plot that value versus rotation rate. At transition points between different regimes, there was a sharp jump in entropy values, while within a given regime entropies varied smoothly, if they varied at all. The biased chaotic state showed a decreasing entropy with increasing rotation rate, as it explored less and less of phase space while moving closer to being locked into the stable doublet state. The doublet state, on the other hand, had entropy which increased with increasing rate, indicating that it explored more of phase space as it moved toward the jump to full chaotic behavior. The en-

tropy of the fully chaotic regime did not vary with rotation rate, indicating that, for a variety of rotation rates, the fully chaotic state explored similar amounts of phase space. This indicates an overall behavior for the fully chaotic state which does not depend on rotation rate within that chaotic regime.

The combination of all of these analysis techniques allowed us to explore a wide variety of interesting behaviors more fully than has been done before. We identified several new types of particle trajectories which had not previously been discussed in the literature, and discovered windows of periodic behavior within a regime which was originally described as a simple chaotic block. Our application of a variety of analysis techniques allowed us to describe these various regimes analytically and provide a measure which can be used to compare these measurements to future work. None of these techniques had been previously applied to experiments in this geometry, and indeed this is the first thorough quantitative analysis of chaotic three-particle dynamics in a rotating drum.

By characterizing the various states that occur within this simple geometry, we have laid a foundation upon which studies of chaos in fluid systems can be based. The rotating drum serves as an ideal model system to which others can be compared. In many ways, this system provides one of the simplest physical fluid dynamical systems in which chaotic behavior can be observed. As a fluid analogue to the classical three-body problem, the drum experiment is of fundamental importance to the understanding of chaos in fluids.

Furthermore, the analysis techniques used in this Dissertation are robust and straightforward to implement, making them a natural starting point for discussing chaotic systems. In addition to the raw numbers, which can be compared outright, the entropy measurements show how behavior varies as we move, with varying rotation rate, between different regimes. Entropy can serve as a predictor of a transition into a regime of distinct behavior, as increasing entropy signaled an approach toward

sharp jumps into states which explored phase space more, and decreasing entropy signaled approaches toward phase transitions into simpler states where phase space was explored less thoroughly. Exploitation of these trends in entropy can serve as a less obvious way of predicting trends, and tuning experiments to seek out interesting or useful regimes.

5.2 Outlook

While we have described a number of new behaviors, and studied the chaotic rotating drum experiment in a depth to which it had not previously been probed, this experiment holds vast potential for future exploration. While we have shown the depth of behavior accessible by simply tuning the rotation rate of the drum, we have not probed the dependence on fluid properties such as Reynolds number. Varying the fluid viscosity, fluid/particle density ratio, or any of a host of other experimental parameters could tell us more about how the fluid dynamics directly affects the chaotic behavior. The question of transient behavior alone deserves significant attention and exploration - we have shown chaotic states that are persistent over many hours, but their behavior in even longer term is as yet unknown. A detailed study, focusing on the approach of final states, and not simply the final states themselves, could reveal even more depth than we have identified. Carrying out these studies of transients would involve some refinements to the experimental apparatus to remove sources of drift, and revisions of the particle tracking algorithm.

Another interesting question is that of dependence on initial conditions. Due to the way the particles were positioned within the drum, it was difficult to control their exact starting positions. A switch to ferromagnetic beads would allow us to use magnets to position the beads wherever we wanted and study how their trajectories evolve. While this still has experimental issues with the lack of accuracy in positioning

the particles and measuring their starting positions, we could gain significant insight into the formation of biased states such as the doublet and biased chaotic states.

Furthermore, we have described how the three-particle system in a rotating drum can demonstrate a rich set of behaviors. Preliminary experiments have demonstrated that the phase diagram of the system can be significantly altered by changes to various parameters. For example, using a longer drum, so that its aspect ratio is larger, and the space available for the beads to explore is greater, results in behavior that almost always settles into the doublet or triplet state, with chaotic states difficult to locate. Similarly, using water in place of pure glycerol results in states which show little chaotic behavior. An ideal direction to take this research would be to vary the fluid properties and look at how various quantities vary not just with rotation rate, but with Reynolds number in general. The fluid viscosity, for example, could be varied over at least an order of magnitude simply by varying the temperature of the heat control bath, as the viscosity of glycerol is highly dependent on temperature. This variation of the fluid dynamical properties would allow us to probe how the chaotic behavior varies not simply with the change of rotation rate, and thus energy supplied to the system, but with the nature of the fluid/particle interactions themselves.

In addition to the interesting new results demonstrated in this Dissertation, the rotating three-body problem holds vast potential for future exploration. Already it serves as a good model system to understand the basics origins of chaotic behavior in fluid systems, and further fleshing out the phase diagram could provide an even more detailed picture of how fluids and particles can interact to produce complicated behavior out of simple geometries.

Bibliography

[1] J. F. Laprise, J. Kroger, H. Kroger, P. Y. Louis, L. J. Dube, E. Endress, A. Burra, R. Zomorrodi, G. Melkonyan, & K. J. M. Moriarty. "Universality of level spacing distributions in classical chaos." (2007).

[2] D. D'Humieres, M. R. Beasley, B. A. Huberman, & A. Libchaber. "Chaotic states and routes to chaos in the forced pendulum." *Physical Review A*, **26**, 3483+ (1982).

[3] P. T. Boyd & S. L. W. Mcmillan. "Chaotic scattering in the gravitational three-body problem." *CHAOS: An Interdisciplinary Journal of Nonlinear Science*, **3**, 507+ (1997).

[4] P. N. Segrè, E. Herbolzheimer, & P. M. Chaikin. "Long-range correlations in sedimentation." *Physical Review Letters*, **79**, 2574+ (1997).

[5] D. J. Tritton. *Physical Fluid Dynamics* (Oxford), 2 edition (1988).

[6] T. M. Verheggen, editor. *Numerical Methods for the Simulation of Multi-Phase and Complex Flow* (Springer, New York) (1992).

[7] K. T. Alligood, T. D. Sauer, & J. A. Yorke. *Chaos: An Introduction to Dynamical Systems* (Springer-Verlag) (1996).

[8] R. Hilborn. *Chaos and Nonlinear Dynamics: An Introduction for Scientists and Engineers* (Oxford University Press, USA) (2000). ISBN 0198507232.

[9] H. Shin & M. R. Maxey. "Chaotic motion of nonspherical particles settling in a cellular flow field." *Physical Review E*, **56**, 5341–5443 (1997).

[10] Anil, Satheesh, & T. R. Ramamohan. "Chaotic dynamics of periodically forced spheroids in simple shear flow with potential application to particle sedimentation." *Rheological Acta*, **34**, 504–511 (1995).

[11] H. Aref & S. Balachandar. "Chaotic advection in a stokes flow." *Physics of Fluids*, **29**, 3515–3521 (1986).

[12] K. Asokan, Anil, J. Dasan, K. Radhakrishnan, Satheesh, & T. R. Ramamohan. "Review of chaos in the dynamics and rheology of suspensions of orientable particles in simple shear flow subject to an external periodic force." *J. Non-Newtonian Fluid Mech.*, **129**, 128–142 (2005).

[13] K. O. L. F. Jayaweera, B. J. Mason, & G. W. Slack. "Behavior of small clusters of spheres falling in a viscous fluid." *J. Fluid Mech*, **20**, 121+ (1964).

[14] I. M. Jánosi, T. Tél, D. E. Wolf, & J. A. Gallas. "Chaotic particle dynamics in viscous flows: The three-particle stokeslet problem." *Physical Review E*, **56**, 2858+ (1997).

[15] E. Ott. *Chaos in Dynamical Systems* (Cambridge University Press) (1993).

[16] C. K. Aidun & J. E. Ding. "Dynamics of particle sedimentation in a vertical channel: Period-doubling bifurcation and chaotic state." *Physics of Fluids*, **15**, 1612–1621 (2003).

[17] I. Kim, S. Elghobashi, & W. A. Sirignano. "Three-dimensional flow over two spheres placed side by side." *J. Fluid Mech.*, **246**, 465–488 (1993).

[18] T. Mullin, Y. Li, D. C. Pino, & J. Ashmore. "An experimental study of fixed points and chaos in the motion of spheres in a stokes flow." *IMA Journal of Applied Mathematics*, **70**, 666–676 (2005). ISSN 0272-4960.

[19] E. R. Weeks. *Experimental Studies of Anomalous Diffusion, Blocking Phenomena, and Two-Dimensional Turbulence*. Ph.D. thesis, The University of Texas at Austin (1997).

[20] B. Cushman-Roisin. *Introduction to geophysical fluid dynamics* (Prentice-Hall) (1994).

[21] M. Lesieur. *Turbulence in fluids* (Kluwer Academic Publishers) (1990).

[22] J. Pedlosky. *Geophysical Fluid Dynamics* (Springer-Verlag, New York, USA), 2 edition (1987).

[23] E. R. Benton & A. Clark. "Spin-up." *Annual Review of Fluid Mechanics* (1974).

[24] H. D. Baehr & K. Stephan. *Heat and Mass Transfer* (Springer) (2006).

[25] P. N. Shankar & M. Kumar. "Experimental determination of the kinematic viscosity of glycerol-water mixtures." *Royal Society of London Proceedings Series A*, **444**, 573–581 (1994).

[26] P. Horowitz & W. Hill. *The Art of Electronics (Second Edition)* (Cambridge University Press), 2nd edition. ISBN 0521498465.

[27] "Pixelink product documentation." `http://www.pixelink.com/support/oem/pixelink\_product\_documentation.htm`.

Appendix A

Video Capture Software

Stream-Pixelink is a rudimentary video streaming capture application which supports the proprietary PixeLINK firewire video camera format, as well as allowing use of the PixeLINK programmable General Purpose Outputs and various other extended features not covered in the IEEE1394 specifications for firewire cameras. In order to use the software, you must install the Pixelink OEM video capture application, as well as the custom written Stream-Pixelink package.

A.1 Software Installation

The software packages used for video capture are installed on the computer TIFFANY in the Weeks lab. If you are using that machine, you can skip software installation and go straight to Sec. A.2. If you need to install the software on any other computers, see the following two Sections.

A.1.1 Pixelink Software

- Download PixeLINK Capture OEM from
  `http://www.pixelink.com/support_software_drivers.asp`
- Run the downloaded install application to install the PixeLINK drivers and

OEM camera capture application.

A.1.2 Installing Stream-Pixelink

- Go to `http://www.physics.emory.edu/~weeks/lab/davidheiser/` and download stream-pixelink-binary.zip.
- Extract the contents of the compressed archive to a convenient location. On the computer TIFFANY in the Weeks lab, the contents are saved in C:\Program Files\Stream-Pixelink\.
- Register the bmptoavi package. In order to use this software, the bmptoavi package *must be registered with the system.* Double click on the batch file reg.bat in the Stream-Pixelink folder to register the package. If it ever necessary to unregister it, unreg.bat can be run.

The source code for Stream-Pixelink is also available at the same URL. Compilation of this source code requires the PixeLINK Software Development Kit (available for purchase at `http://www.pixelink.com` and stored in C:\james on TIFFANY). and Microsoft Visual Studio 2008. The PixeLINK SDK is installed on TIFFANY under C:\Program Files\PixeLINK\.

To compile the code, open the Visual Studio solution Stream-Pixelink.sln in Visual Studio and select Build → Build Solution.

Note that many options are hard coded into the program, and thus the code must be recompiled to change those options. The most significant of these is the recording frame rate. By default, the code records video at five frames per second, and the code must be recompiled to change this option. This default value was chosen because 5fps is a number we know from experience can be streamed with little or no dropped frames on the computer TIFFANY. Most important options are defined within stream-pixelink.cpp.

A.2 Setting up the PixeLINK IEEE1394 Camera

Most of the camera options are set up within the PixeLINK Capture OEM software. By default, the software may load the "basic" view, shown in Fig A.1a. If so, first switch to the "advanced" view by clicking View → Advanced Mode

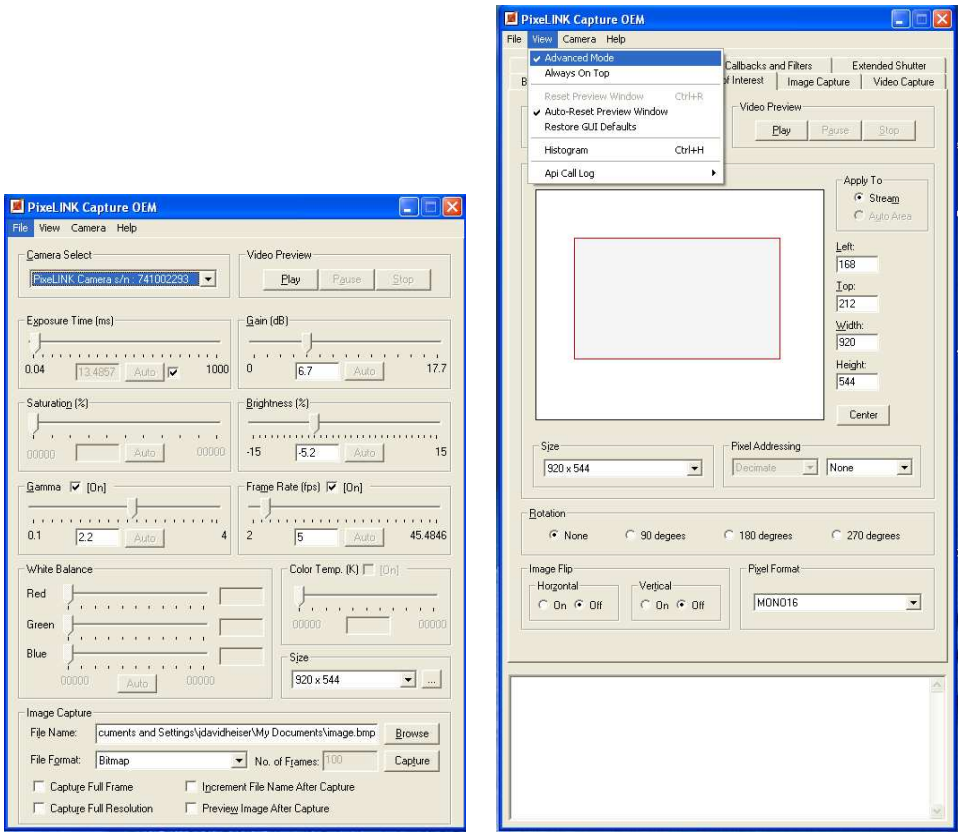

(a) "basic" view (b) "advanced" view

Figure A.1: Pixelink Capture OEM defaults to a simple interface. Many of the options we need to access are only available in the "advanced" mode.

The advanced mode of the PixeLINK Capture OEM software is organized with a number of tabs along the top of the window. Three of these are of interest to us - Basic Controls, Region of Interest, and External Control.

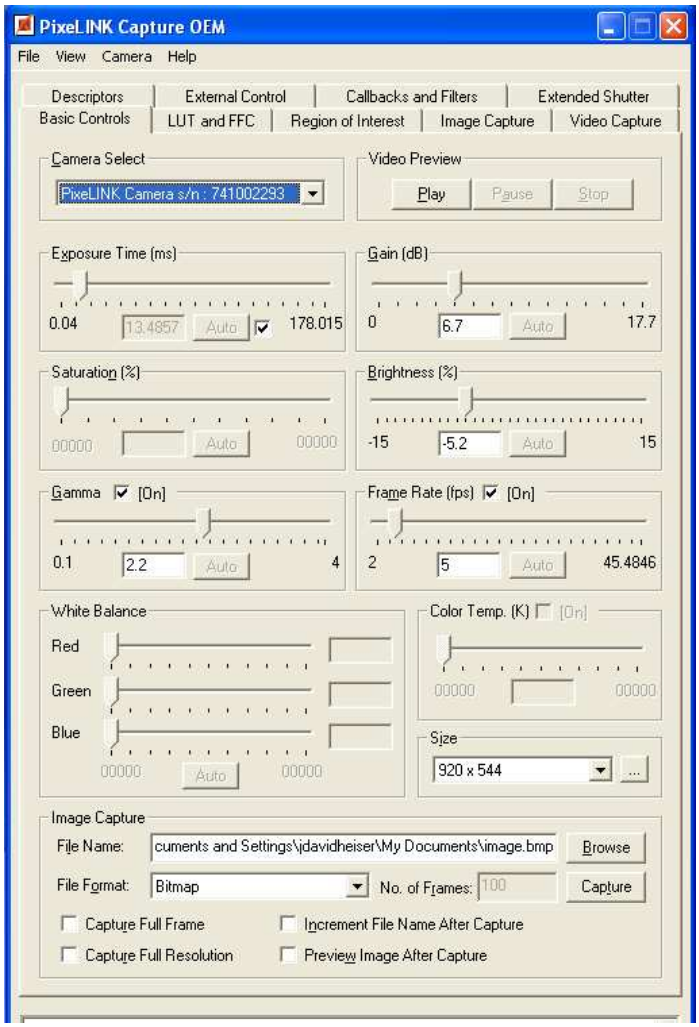

Figure A.2: The Basic Controls tab contains typical camera settings such as Brightness and Exposure Time

A.2.1 Basic Controls Tab

The basic controls tab contains typical camera control options. The Exposure Time, Saturation, Brightness, Gain, and Frame Rate can all be adjusted here. Note, however, that the frame rate will be reset by Stream-Pixelink.

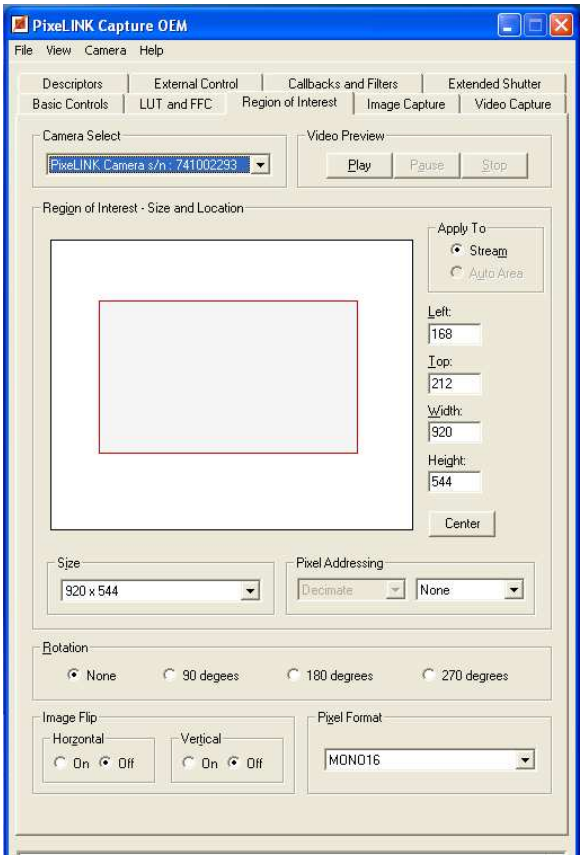

Figure A.3: The ROI tab contains controls for the camera Region of Interest

A.2.2 Region of Interest Tab

The Region of Interest tab contains settings to control the recorded ROI for the camera. Limiting the ROI allows us to save storage space and streaming bandwidth by only recording the region of the image which is important for our experiment. Since the aspect ratio of the drum is different from the typical 4:3 ratio of the CCD sensor in the camera, it is useful to set a region of interest which matches the aspect ratio of the experiment. Here the pixel format of the video stream can also be set - MONO16 seems to work best with the compression algorithms used in Stream-Pixelink. Furthermore, this tab allows the video to be flipped or rotated, if needed.

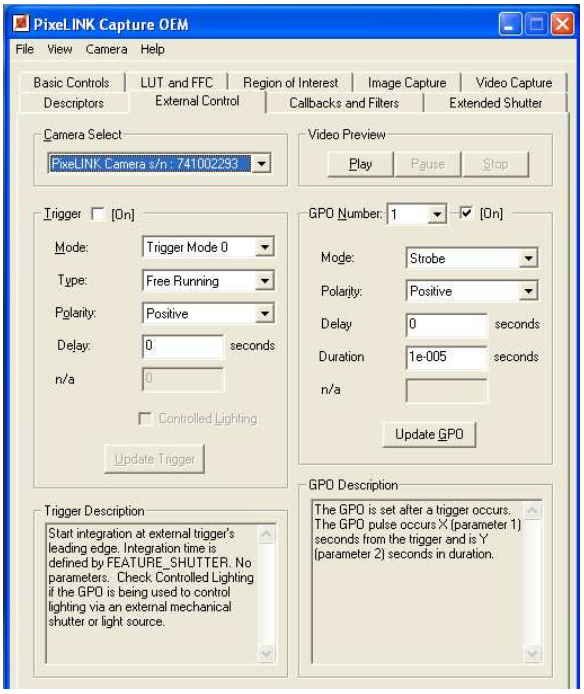

Figure A.4: The External Control tab sets options for camera input and output

A.2.3 External Control Tab

The External Control tab contains controls for the camera's input trigger and General Purpose Output. The GPO is used to control the Nova-Strobe as described in Sec. 3.1.3. In order to have the strobe fire with each frame of the video, the following options should be set:

GPO Number: 1 (check box checked to turn the GPO on)

Mode: Strobe

Polarity: Positive

Delay: 0 seconds

Duration: 1e005 seconds.

After enabling the appropriate options, press the UPDATE GPO button to update these options to the camera. Note that all options will be lost if the camera loses power. This includes unplugging the camera from the PC, or turning off the PC.

A.3 Running Stream-Pixelink

The code can be run in two ways. By double clicking on the program Stream-Pixelink.exe in Explorer, you can run the code with the default number of frames (5fps∗3600s/h∗6h, a six hour long movie). If you want to define your own number of frames, Stream-Pixelink must be run from a DOS command prompt.

Open a DOS command prompt by clicking START → RUN and typing in CMD, then pressing OK.

Navigate to the directory where Stream-Pixelink is stored. If Stream-Pixelink is stored in C:\Program Files\Stream-Pixelink\, type

```
cd  C:\Program Files\Stream-Pixelink\
```

The structure of the command to run Stream-Pixelink is simply

```
Stream-Pixelink [number of frames]
```

So to capture a movie with 100 frames, you would type

```
Stream-Pixelink 100
```

at the DOS command prompt and press enter.

On launch, Stream-Pixelink will first pop up a prompt asking for a location and filename. Be sure to include .avi at the end of your filename, as the program does not add this extension by default.

After this command prompt, Stream-Pixelink will ask for the compression settings to use in creating the video file, as seen in Fig. A.3. In our testing, we found that the Xvid algorithm performed well for streaming data directly to disk without dropping many frames. Once you select a compression and press OK, Stream-Pixelink will begin capturing video.

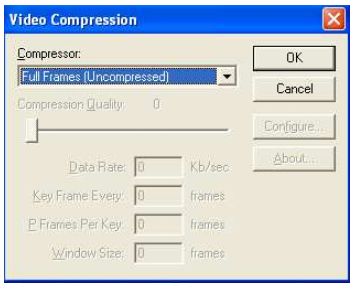

Figure A.5: Stream-Pixelink pops up a dialog to select the compression algorithm to be used. In our testing, the Xvid algorithm, with default settings, performed well.

Note that Stream-Pixelink is *not* a multi-threaded application. What this means is that the application can only do one thing at once. Thus, if you move the windows around while Stream-Pixelink is capturing video, the acquisition of frames will halt while you move the windows. This will lead to dropped frames. *Do not move any windows around while Stream-Pixelink is capturing data.*

While Stream-Pixelink is running, there will be a text window showing warnings if any frames are dropped. There will also be a cancel dialog. Clicking CANCEL within this dialog will interrupt the video acquisition, finalize the video file, and exit the program. If the cancel button is not pressed, Stream-Pixelink will automatically exit when acquisition of the prescribed number of frames is completed.

Appendix B

Video Tracking Software

TrackMovieSeq is a Matlab package which reads video file from any windows-readable format and analyzes the contents. This allows significant storage space savings, as data to be analyzed can be stored as a compressed movie file and read frame-by-frame for analysis

B.1 Software Installation

The Matlab packages used for video analysis are installed on the computer TIFFANY in the Weeks lab under C:\james\trackmovie. If you need to install the files on any other computers, go to `http://www.physics.emory.edu/~weeks/lab/davidheiser/` and download trackmovie.zip. Extract the contents to a convenient location.

B.2 TrackFramebeta.m

OUTPEAKS = TrackFrameBeta(FOO,DEBUG) is a package to carry out particle tracking on a single RGB bitmapped image. FOO is the input image to be tracked, and DEBUG is an optional flag to produce debugging images. DEBUG= 1 will produce several plots showing the various stages of the tracking algorithm, while DEBUG= 2 will

produce a single image, with tracked points overlaid on the original image. Tracked points are returned as a struct comprised of two column vectors. OUTPEAKS.X contains x values, and OUTPEAKS.Y contains y values.

Trackframebeta has many hard-coded options which are optimized for the particular rotating drum experiment discussed in this Dissertation. Specifically, it has a check to ensure that three particles are found, and it has tolerances set to correspond with the lighting used in this experiment. If different lighting or numbers of particles are used, these options will need to be modified.

B.3 TrackMovieSeq.m

TRACKMOVIESEQ(FILENAME,FRAMES,DEBUG) is the package to evaluate entire movies. This package uses PROCESSFRAME-TRACK.M to analyze individual frames from the video stream, extracting each frame as an uncompressed bitmap, passing it to TRACKFRAMEBETA, and saving the results. After execution, the program automatically saves all variables to a timestamped .MAT file named after the original video. The main important variables, X and Y,are 3-column vectors of positions for each particle.

FILENAME is the name of the file to be analyzed. FRAMES gives a selection of frames within the movie to be analyzed, so, for example
TRACKMOVIESEQ(TEST.AVI,[1000:2000]) would analyze frames 1000 through 2000 in the file test.avi.

DEBUG is again an optional debug parameter, to be passed to TRACKFRAMEBETA, with the same possible values.